Development and Implementation of a Preconditioner for a Five-Moment One-Dimensional Moment Closure

by

Amir Reza Baradaran Hosseini

Thesis submitted to the
Faculty of Graduate and Postdoctoral Studies
In partial fulfillment of the requirements
For the M.A.Sc. degree in
Mechanical Engineering

School of Mechanical Engineering
Faculty of Engineering
University of Ottawa

Abstract

This study is concerned with the development and implementation of a preconditioner for a set of hyperbolic partial differential equations resulting from a new 5-moment closure for the prediction of gas flows both in and out of local equilibrium. This new 5-moment closure offers a robust and efficient system of first-order hyperbolic partial differential equations that has proven to provide an accurate treatment of one-dimensional gases, both in and for significant departures from local thermodynamic equilibrium. However, numerical computations using this model have proven to be difficult as a result of a singularity in the closing flux of the system. This also causes infinitely large wavespeeds in the system. The main goal of this work is to mitigate these numerical issues. Since the solution of a hyperbolic system is characterized by the waves of the system, one could suggest to scale these wavespeeds to remove the arbitrarily large speeds without altering the solution of the system. To accomplish this, this work starts with a detailed study of the behaviour of the system's wavespeeds, given by the eigenvalues of the flux Jacobian of the system. Since, it is not possible to solve for these eigenvalues explicitly, it is suggested to approximate them by interpolation between the few states at which these waves can be solved for explicitly. With an estimate for the wavespeeds, the nature of the singularity in the system can be analyzed mathematically. The results of this mathematical analysis are used to develop a preconditioner matrix to remove the singularity from the model. To implement the proposed preconditioned model numerically, a centred-difference scheme with artificial dissipation is proposed. A dual-time-stepping strategy is developed and implemented with implicit Euler time marching for both physical and pseudo time iteration. This dual-time

treatment allows the preconditioned system to remain applicable to time-accurate problems and is found to greatly increase the robustness of the solution of the steady-state problems. Solutions to several canonical problems for both continuum and non-equilibrium flow are computed and comparisons are made to classical models.

Acknowledgements

I would like to thank my friends and family for their support during my studies. I am especially grateful of the support and encouragement that my parents have offered me over the years. They have always been there for me and give their support and love for everything I have pursued during my life.

I feel privileged to have had the opportunity to continue my education at the University of Ottawa Department of Mechanical Engineering. During my program, I was lucky to work with an amazing group of professors and colleagues.

I would like to thank my thesis advisor, Professor James McDonald, for his support, guidance and encouragement that made this made this thesis possible. He has shared his knowledge for the field of moment closure and computational fluid dynamics with me over my program and given every opportunity to take part in the research community. I am also grateful to him for his financial support.

Amir Reza Baradaran

University of Ottawa Department of Mechanical Engineering

January 2015

Table of Contents

List of Figures

Chapter 1

Introduction

1.1 Moment Closures

Traditionally, the Euler equations are used to describe the time evolution of a gas in local thermal equilibrium. In this regime, it is considered as an accurate model. The famous compressible Navier-Stokes equations, which are extremely widely used, are a reliable model when there are only very small deviations from this local equilibrium. The degree to which a gas deviates from local equilibrium can be defined through the definition of the flow Knudsen number,

$$Kn = \frac{\lambda}{l}\,. \tag{1.1}$$

Here, the mean free path, λ, is the average distance that a gas particle travels between each collision with other particles and l is a length scale that characterizes the flow problem. A small Knudsen number means gas-particle collisions happen frequently over the length of the problem. The result is that the flow remains very near local thermodynamic equilibrium. These flows are said to exist in the continuum regime, where the Navier-Stokes equations provide an accurate model. Despite the accuracy of the model in this region, it has been shown that the Navier-Stokes equations suffer from several mathematical

and numerical problems related to the second-order derivatives used to treat viscous and heat-transfer effects. These issues include physical problems, such as the Navier-Stokes equation's prediction of infinite speeds of information propagation [23], as well as computational limitations, such as the difficulty of finding discrete representation of second derivatives on practical irregular meshes that are both accurate and positive [6, 20].

When the Knudsen number becomes larger, particle interactions occur more infrequently and deviations from local equilibrium become significant. When this happens, neither of the two classical models discussed above can make accurate predictions. Such non-equilibrium gas flows include micro-scale flows, highly rarefied flows, very high-speed flows and many other flows with extreme gradients in fluid properties.

The most widely used method in this non-equilibrium regime is the direct simulation Monte Carlo (DSMC) method established by Bird [2]. In this model, one needs to make use of an extremely large number of representative particles to represent real molecules. The evolution of these representative particles is modeled in a statistical way that is expensive and has very slow error convergence. Although the Monte Carlo model is believed to be valid for all Knudsen numbers, its practical applicability is limited by its slow convergence rate, especially for flows with a high number of particles or for low-speed flows. The DSMC method is widely used for situations when the Knudsen number is above 10, the method tends to become prohibitively expensive for values below that. Other methods that remain valid for all Knudsen numbers are based on direct numerical discretization of the high-dimensional Boltzmann equations [22]. These methods also suffer from computational cost caused by solving partial differential equations (PDEs) in a seven-dimensional phase space.

Typically, flows can be divided into three separate regimes based the on the Knudsen number. This separation is shown in Table 5.1.

Table 1.1: **Definition of Gas-Flow Regimes**

$0 < \text{Kn} \leq 0.01$	Continuum Regime
$0.01 < \text{Kn} < 10$	Transition Regime
$10 \leq \text{Kn}$	Free-Molecular Regime

Many practical flows exist in the continuum and transition flow regimes. A model that remains both physically valid and computationally efficient across this regime is therefore desirable. Moment closures, derived from the Boltzmann equation, have been shown to be capable of producing such models. The promise of more accurate and affordable predictions of flow behaviour in the transition regime, where the Navier-Stokes equations are not accurate, and a less complex set of hyperbolic PDEs involving only first derivations make moment closures an attractive alternative to the traditional methods. Also, the requirement of solving only first derivatives means numerical solution of systems of moment equations can be more convenient than solving traditional models, even in the continuum regime. [20].

Unfortunately, traditional moment closures have suffered from their own limitations. The original closure hierarchy, suggested by Grad [11], does not guarantee the state of the gas remains physically realistic, even for small deviations from local-equilibrium conditions. The resulting models are often ill-posed for realistic initial boundary value problems. Likewise, the other most widely used hierarchy of moment closures, the maximum-entropy hierarchy, produces models that are undefined and singular for some physically realistic moment states whenever heat transfer is included in the model [13]. The result of this singularity in the model is that fluxes and wavespeeds in the system can be infinite. Though

these maximum-entropy closures can be proven to remain hyperbolic, physically realizable, and well-posed for all realistic states when the system is not singular, fluxes cannot be written in closed-form and must be determined through the numerical solution of an expensive entropy-maximization problem whenever needed.

Recently, a new moment closure of the Boltzmann equation was presented by McDonald and Torrilhon [21]. It is based on an approximation of the maximum-entropy hierarchy. The goal of this new idea is to provide a robust and efficient model over the continuum and the transition regimes (Kn < 10). The new model remains physically valid and well-posed even for significant deviations from local equilibrium. The PDEs resulting from the model also remain strictly hyperbolic over the range of physically realizable states. Besides the enhanced physical validity of the new model, the first-order balance-law structure of the PDEs bring many computational and mathematical advantages [19]. However, the new model maintains one feature of the original maximum-entropy model that is difficult to deal with in practice. It maintains a singularity in the flux vector for some realizable moment states. This singularity was intentionally preserved as it was found to be an important component that leads to very physically accurate predictions, however it can be difficult to control numerically. In order to overcome this problem, a new preconditioning strategy is developed, implemented and validated in this current work.

1.2 Objectives of the Current Study

The objective of the current study is to develop a preconditioner matrix to overcome the problem of infinitely large wavespeeds in the moment system, since the existence of these

wavespeeds lead to difficulties in numerical computation and can make numerical solution impossible in some cases. In order to obtain the preconditioner, one needs to investigate the behaviour of the wavespeeds of the recently proposed model for a one-dimensional situation over the whole physically realizable domain. To do this, the five wavespeeds of the one-dimensional system—the roots of the characteristic equation given by a flux-Jacobian matrix of the system—need to be found. The characteristic equation is shown to be a quintic polynomial and, as the roots of a quintic polynomial cannot be written in closed form, the wavespeeds of the system cannot be found explicitly. To overcome this, an expression is suggested for each wavespeed which is shown to give a very accurate approximation for the real wavespeeds across the range of possible states. Knowledge of these wavespeeds, particularly how they behave near the singularity, is used to construct an appropriate preconditioner. The proposed preconditioner is implemented in the model and the preconditioned system is solved for several cases. Solutions derived from the preconditioned system are then compared with ones from the original system for same cases in order to validate the proposed preconditioner. Comparisons are made to other classical models in order to demonstrate the advantages of the moment-based system.

1.3 Scope of the Current Study

This study begins, in Chapter 2, with a brief introduction to gaskinetic theory. Special attention is given toward to the field of moment closures. Traditional Grad and maximum-entropy closures are introduced and some of their limitations are presented. Thereafter, a new closed-form moment closure including five PDEs for a one-dimensional gas is shown. In

Chapter 3, the five wavespeeds of the one-dimensional system are analyzed and an accurate approximation is found for each. The technique of preconditioning is introduced and, based on the presented approximate wavespeeds, a preconditioner matrix is suggested for the one-dimensional system that removes the singularity in the flux but does not change the steady-state solution of the original system. Chapter 4 includes techniques that are used for solving the preconditioned system numerically and techniques to speed up the convergence rate of these solutions. Results of numerical solutions of several different problems, solved with the preconditioned system, are presented in Chapter 5. In some cases these results are compared with results computed using the original non-preconditioned system, the Navier-Stokes equations and the exact solutions. Finally, the last chapter concludes with a summary of achievements and recommendations for future studies.

Chapter 2

Review of Gaskinetic Theory

2.1 Kinetic Theory

Traditional fluid dynamical descriptions of gases are based on the small-Knudsen-number assumption, meaning the gas remains very close to local thermal equilibrium and the evolution of fluid properties (mass density, fluid velocity, pressure and temperature) is well described by either the compressible Euler or Navier-Stokes equations [17, 10].

However, when this assumption is not valid, and the distance each particle travels between particle collisions become large enough, a new model is needed to describe gas behaviour. Kinetic theory of gases can be used to fill this need. One objective of the kinetic theory is to describe the macroscopic properties of gases; such as pressure, temperature, thermal conductivity, and viscosity; using microscopic quantities that are associated with the molecules that compose the gases; such as particle mass, velocity, kinetic energy, internal degrees of freedom and interaction forces between the molecules [14, 10]. As kinetic theory provides a direct treatment for gas-particle behaviour, it can be used to construct models that are valid for any range of Knudsen number. Kinetic theory assumes that a gas is composed of a very large number of identical particles, typically 2.43×10^{16} per cubic mil-

limeter at standard conditions (1 bar, 25 °C), moving independently of each other. These particles interact through collisions and, despite their small size, they are assumed to still follow the laws of classical mechanics. This approach has led to a general description of gas properties based on the time-evolution of a non-negative distribution function that defines the distribution of particle velocities as a function of space and time [13]. Macroscopic properties of a gas; such as density, velocity, pressure and heat flux; are mathematical moments of this distribution function.

2.2 The Velocity Distribution Function

In kinetic theory, the density of particles with microscopic velocity, v_i, at time, t, and position, x_i, is defined by a distribution function, $\mathcal{F}(x_i, v_i, t)$. This distribution function is defined such that [26]

$$N_{x_i,v_i} = \mathcal{F}(x_i, v_i, t)\mathrm{d}x_i\mathrm{d}v_i\,, \tag{2.1}$$

where N_{x_i,v_i} gives the number of particles existing in a six-dimensional phase space with velocities between the range of v_i and $v_i + \mathrm{d}v_i$ located in a space interval of x_i and $x_i + \mathrm{d}x_i$ at time t. As it can be seen in Figure 2.1, for a one-dimensional gas (one space dimension and one velocity dimension), $N_{x,v}$ is the number of particles that are surrounded by $\mathrm{d}v$ and $\mathrm{d}x$ for velocity v and space location x.

Integrating Equation (2.1) over all possible velocities and locations gives the total number of particles composing a gas,

$$N = \int_V \int_X \mathcal{F}(x_i, v_i, t)\mathrm{d}x_i\mathrm{d}v_i\,. \tag{2.2}$$

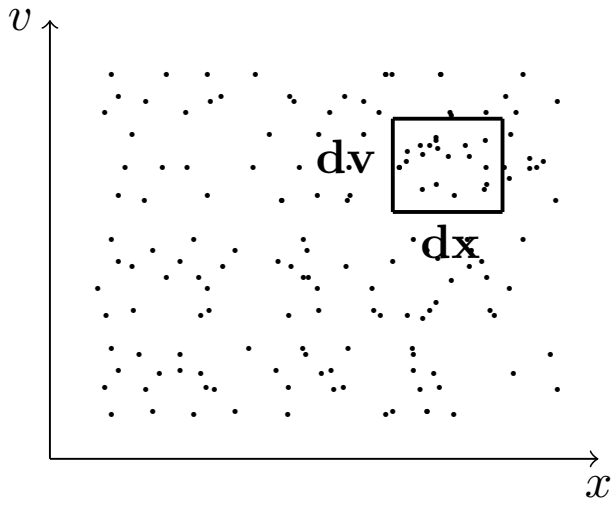

Figure 2.1: *Representation of the two-dimensional phase space and a differential cell of phase space for a one-dimensional gas. Each dot represents the momentary state of one particle.*

This assumes the total number of gas particles in the system does not change with time. Similarly, the number density of particles, $n(x_i, t)$, can be obtained by integrating the distribution function only over velocity space,

$$n(x_i, t) = \int_V \mathcal{F}(x_i, v_i, t) \mathrm{d}v_i \,. \tag{2.3}$$

It is often common to define the normalized phase-space distribution function by

$$f(x_i, v_i, t) = \frac{\mathcal{F}(x_i, v_i, t)}{n(x_i, t)} \,, \tag{2.4}$$

such that its integral over velocity space is always equal to 1.

2.2.1 The Maxwell-Boltzmann Distribution

A simple argument by Maxwell allows us to find the normalized phase-space distribution function that describes a gas in local thermal equilibrium [4]. In such situation, the velocity distribution function, known as the Maxwell-Boltzmann distribution, is defined uniquely

by its temperature, T, density, ρ, and average velocity, u_i, as [18]

$$\mathcal{F}(x_i, v_i, t) = n \left(\frac{\beta(x_i, t)}{\pi} \right)^{(\frac{3}{2})} \exp^{\left(-\beta(x_i,t)(v_i-u_i)^2\right)} . \tag{2.5}$$

Here, β is given by

$$\beta(x_i, t) = \frac{m}{2} \kappa T(x_i, t) , \tag{2.6}$$

where $\kappa = 1.38053 \times 10^{-3} \frac{J}{K}$ is the Boltzmann constant, m is the particle mass and $T(x_i, t)$ is the temperature of the fluid at location, x_i, and time, t. Maxwell's five basic assumptions used to find the equilibrium state can be summarized as [10]:

- The gas is composed of an indefinite number of small hard spheres acting on one another through collisions.
- The direction of a particle's velocity has an equal probability over all solid angles after a collision.
- The distribution of molecular velocities is independent of time in equilibrium.
- The distribution function is isotropic in equilibrium.
- The orthogonal components of the molecular velocities are statistically independent after a large number of collisions.

It has been proven that a gas at any non-equilibrium state will always move toward the Maxwell-Boltzmann distribution due to particle collisions and, after reaching that state, particle collisions no longer have any effect on the distribution function [10].

2.2.2 Moments of the Distribution Function

As mentioned before, macroscopic properties of a gas (mass density, velocity, etc.) are moments of the distribution function integrated over particle-velocity space. In order to calculate these properties, velocity moments need to be taken. This means multiplying the distribution function by an appropriate velocity weight, $M(v)$, and integrating over all velocity space. For instance, mass density, ρ, can be calculated by

$$\rho = mn = \iiint_{\infty} m\mathcal{F}(x_i, v_i, t)\mathrm{d}^3 v_i = \langle m\mathcal{F} \rangle \ , \tag{2.7}$$

where the molecular mass, m, of the gas is being taken as the weighting function. The notation, $\langle M(v_i)\mathcal{F} \rangle$, is used to denote integration over the whole velocity space. Similarly, the momentum density of the gas also can be calculated by

$$\rho u_i = m \iiint_{\infty} v_i \mathcal{F}\mathrm{d}^3 v_i = \langle m v_i \mathcal{F} \rangle \ . \tag{2.8}$$

Here, u_i denotes the bulk or mean velocity, while v_i is the individual particle velocity. Using the definitions of mass density and momentum density, one can define the bulk velocity by

$$u_i = \frac{1}{n} \iiint_{\infty} v_i \mathcal{F}\mathrm{d}^3 v_i = \frac{\langle v_i \mathcal{F} \rangle}{n} \, , \tag{2.9}$$

or

$$u_i = \frac{\langle m v_i \mathcal{F} \rangle}{\langle m \mathcal{F} \rangle} \, . \tag{2.10}$$

At this point, a new velocity, the random velocity, c_i, is also defined to show the speed of the particles as measured by an observer moving with the gas's mean velocity

$$c_i = v_i - u_i \, . \tag{2.11}$$

Using the random velocity, higher-order moments which define some important physical properties such as pressure and heat flux can be computed. For example, a second-order pressure tensor is defined by

$$P_{ij} = m \iiint_{\infty} c_i c_j \mathcal{F} \mathrm{d}^3 c = \langle m c_i c_j \mathcal{F} \rangle \ . \tag{2.12}$$

The pressure tensor is related to the thermodynamic pressure by

$$p = \frac{1}{3} P_{ii} \, . \tag{2.13}$$

It is related to the deviatoric "viscous" stresses as

$$\tau_{ij} = \delta_{ij} p - P_{ij} \, . \tag{2.14}$$

Similar to the pressure tensor, the generalized heat-flux tensor is defined by

$$Q_{ijk} = m \iiint_{\infty} c_i c_j c_k \mathcal{F} \mathrm{d}^3 c = \langle m c_i c_j c_k \mathcal{F} \rangle \ . \tag{2.15}$$

The traditional heat-flux vector is related to this third-order tensor as

$$q_i = \frac{1}{2} Q_{ijj} = \frac{1}{2} \langle m c_i c_j c_j k \mathcal{F} \rangle \ . \tag{2.16}$$

2.3 The Boltzmann Equation

As discussed before, the time evolution of a distribution function defining a gas is described by the Boltzmann equation [10, 13, 26]. It can be written as

$$\frac{\partial \mathcal{F}}{\partial t} + v_i \frac{\partial \mathcal{F}}{\partial x_i} + \frac{\partial}{\partial v_i} \left(a_i \mathcal{F} \right) = \frac{\delta \mathcal{F}}{\delta t} \, . \tag{2.17}$$

The last term of the left-hand side of the equation is related to particle acceleration, a_i, caused by external forces. In the current work, for simplicity's sake, the acceleration term is taken to be zero. The non-linear collision operator term, $\frac{\delta \mathcal{F}}{\delta t}$, on the right-hand side of the equation represents the effects of particle collisions on the velocity distribution function. Evaluating the collision operator is difficult, as it involves a complex five-dimensional integral. More details about the collision operator are given in the next section.

2.3.1 The Collision Operator

Particle collisions involve momentum and energy exchange between particles. These exchanges cause the distribution function, $\mathcal{F}$, to change with time. As a result, in order to solve the Boltzmann equation, detailed information is required regarding these particle interactions. In order to model these collisions, several assumptions must be made. First, it is assumed that only binary collisions occur. It is also assumed that there is a large enough number of particles so that no single collision can change the distribution function appreciably and that the distribution function is constant in space over the range of interaction potential forces between particles. Finally, it is assumed that particle velocities are uncorrelated. Using these assumptions and the laws of classical mechanics, it can be proven that the collision operator has a form

$$\frac{\delta \mathcal{F}}{\delta t} = \int_V \int_0^{2\pi} \int_0^{\frac{\pi}{2}} \left(\mathcal{F}' \mathcal{F}^{1\prime} - \mathcal{F} \mathcal{F}^1 \right) g \sigma \sin\theta \mathrm{d}\theta \mathrm{d}\epsilon \mathrm{d} {v_i}^1 \,, \tag{2.18}$$

where,

$$\mathcal{F} = \mathcal{F}(x, v_i, t), \qquad \mathcal{F}^1 = \mathcal{F}(x, {v_i}^1, t), \qquad \mathcal{F}' = \mathcal{F}(x, {v_i}', t), \qquad \mathcal{F}^{1\prime} = \mathcal{F}(x, {v_i}^{1\prime}, t) \,.$$

Here, v_i and ${v_i}^1$ are the velocities of two independent particles before a collision, similarly ${v_i}'$ and ${v_i}^{1\prime}$ are the corresponding velocities for those particles after an interaction. In Equation (2.18), the relative speed of the particles prior to the collision is given by g, $g = v_i - {v_i}'$, σ is the differential collision cross section of a particle, θ is the deflection angle, and ϵ shows a solid angle. A graphical representation of a single collision is shown in Figure 2.2. More details about the derivation of the collision operator integral can be found in any standard kinetic-theory textbook [10, 26].

In general, the collision operator is high-dimensional, complicated, and difficult to handle in practice. Therefore, simplified models are widely used to model the effects of particle interactions. One of the most common models developed was suggested by Bhatnagar, Gross and Krook (BGK) in 1954 [1]. In this model, it is assumed that particles corresponding to a non-equilibrium state are removed and equilibrium-state particles are added on prescribed time scales,

$$\frac{\delta \mathcal{F}}{\delta t} = -\frac{\mathcal{F}\left(x_i, v_i, t\right)}{\tau_{\mathcal{F}}\left(x_i, t\right)} + \frac{\mathcal{M}\left(x_i, v_i, t\right)}{\tau_{\mathcal{M}}\left(x_i, t\right)}\,. \tag{2.19}$$

Now, the equilibrium Maxwellian distribution is denoted by $\mathcal{M}\left(x_i, v_i, t\right)$. The time scale on which non-equilibrium particles are removed is $\tau_{\mathcal{F}}$ and the time scale on which equilibrium particles are added is $\tau_{\mathcal{M}}$. In this study, these times are taken to be equal to ensure conservation of particles.

2.4 Moment Closures

The computational cost of a direct solution of the Boltzmann equation has proven to be prohibitive. This is because schemes that are used to solve the Boltzmann equation

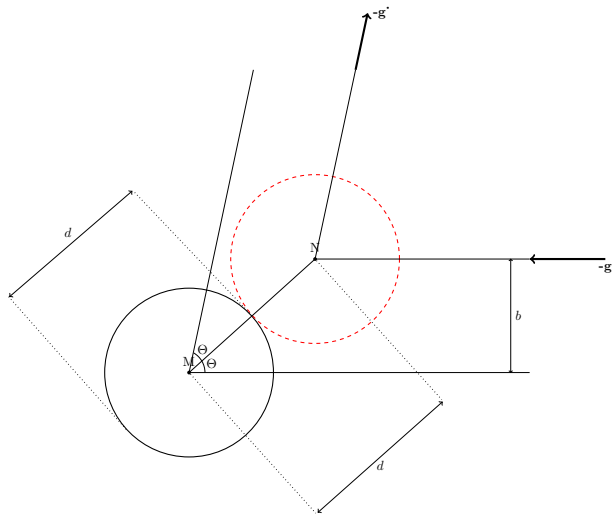

Figure 2.2: *Collision of two hard spheres of diameter d.*

numerically require a discretization of the physical spacial domain of the problem as well as a disretization of the infinite domain of velocity space with sufficient resolution to accurately represent the velocity distribution function of the gas particles for the entire flow domain [18]. Beside that, for most practical applications, most of the information derived from solving the Boltzmann equation is unnecessary. As a result, a simpler and more practical method is desired. The method of moment closure, derived from the Boltzmann equation, promises an alternative method to describe a monatomic gas's behaviour as compared to traditional techniques, such as the Euler or Navier-Stokes models.

The theory of moment closures comes from the realization that the detailed information regarding the exact microscopic state of a gas is usually not important in the end. Rather, it is the macroscopic moments of the gas that are generally of interest. In this method, a set of hyperbolic partial differential equations for the evolution of moments of the gas can be derived by taking moments of the Boltzmann equation,

$$\frac{\partial}{\partial t}\left\langle mM^N(v_i)\mathcal{F}\right\rangle + \frac{\partial}{\partial x_i}\left\langle mv_iM^N(v_i)\mathcal{F}\right\rangle + \frac{\partial}{\partial v_i}\left\langle ma_iM^N(v_i)\mathcal{F}\right\rangle = \left\langle mM^N(v_i)\frac{\delta\mathcal{F}}{\delta t}\right\rangle . \quad (2.20)$$

Here, $M^N(v_i)$ indicates the chosen velocity weight corresponding to the moment of interest. As before, particle acceleration due to external fields is assumed to be zero in the present work. Therefore, Equation (2.20) can be rewritten as

$$\frac{\partial}{\partial t}\left\langle mM^N(v_i)\mathcal{F}\right\rangle + \frac{\partial}{\partial x_i}\left\langle mv_iM^N(v_i)\mathcal{F}\right\rangle = \left\langle mM^N(v_i)\frac{\delta\mathcal{F}}{\delta t}\right\rangle . \tag{2.21}$$

Typically, one is not simply interested in one moment, but rather a set of moments. Therefore, a new notations is defined such that

$$\mathbf{M} = \left[M^0(v_i), M^1(v_i), ..., M^N(v_i)\right]^T , \tag{2.22}$$

where $\mathbf{M}$ is a column vector including different weights corresponding to the moments of interest. Here, N is the number of the entries in the vector. Using this vector, moment relations can be written in the vector form as

$$\mathbf{U} = \left\langle m\mathbf{M}\mathcal{F}\right\rangle . \tag{2.23}$$

Here, $\mathbf{U}$ is the moment vector containing all the moments of the interest for a practical application. One can rewrite Equation (2.21) in vector form as

$$\frac{\partial \mathbf{U}}{\partial t} + \frac{\partial}{\partial x_i}\left\langle mv_i\mathbf{M}\mathcal{F}\right\rangle = \left\langle m\mathbf{M}\frac{\delta\mathcal{F}}{\delta t}\right\rangle . \tag{2.24}$$

Introducing the flux dyad, $\mathbf{F}_i = \left\langle mv_i\mathbf{M}\mathcal{F}\right\rangle$, and $\Delta\left[\mathbf{M}\mathcal{F}\right] = \left\langle m\mathbf{M}\frac{\delta\mathcal{F}}{\delta t}\right\rangle$ as the effect of microscopic collisions on the macroscopic moments, Equation (2.24) is written as

$$\frac{\partial \mathbf{U}}{\partial t} + \frac{\partial \mathbf{F}_i}{\partial x_i} = \Delta\left[\mathbf{M}\mathcal{F}\right] . \tag{2.25}$$

Equations (2.25) is often referred to as Maxwell's equation of change, and provides a

description of the time evolution of macroscopic properties of a gas. It can be seen that solving $\mathbf{U}$ is dependent on $\mathbf{F}_i$, while $\mathbf{F}_i$ always includes moments of one order higher than those in $\mathbf{U}$, in terms of the velocity [18]. In order to solve the system of equations, one could suggest to write an infinite number of moment equations to describe the time evolution of any macroscopic quantity, however, this is obviously impossible. A better idea is to write a finite number of moment equations by artificially closing the system in some way. One technique to write a closed system of moment equations is to restrict the distribution function to have a prescribed form. The number of free parameters, in the prescribed distribution function, $\boldsymbol{\alpha} = [\alpha_1, \alpha_2, ..., \alpha_n]^T$, must be the same as the number of entries in the vector $\mathbf{U}$. Once these parameters are chosen such that Equation (2.23) is satisfied, any needed higher order moment can be directly integrated and the system is closed.

2.4.1 The Grad Closure Hierarchy

Restricting the distribution function to close the moment system was first suggested by Grad in 1949 [11]. His suggestion was to use a polynomial expansion around the equilibrium Maxwellian as a restricted distribution,

$$\mathcal{F}\left(x_i, v_i, t\right) = \mathcal{M}\left(x_i, v_i, t\right) \boldsymbol{\alpha}^T \mathbf{M}\,. \tag{2.26}$$

Here, $\mathbf{M}$ is the vector that includes the generating weights and generally contains monomials of the particle velocity, v_i. The vector of coefficients of the distribution function, $\boldsymbol{\alpha}$, are chosen such that the moments in the solution vector, $\mathbf{U}$, satisfy Equation (2.23) [19]. Despite having a closed set of transport equations for a finite set of velocity moments, the resulting distribution function in Grad-type moment closures can be negative, which is not

physically realistic (one cannot have a negative number of particles at any location in phase space). More devastating is the fact that, even for small deviations of local equilibrium, Grad's moment closures lose hyperbolicity and yield moment equations that are ill-posed for many initial value problems [29, 30]. This happens when the Jacobian of the flux vector develops complex eigenvalues.

2.4.2 Maximum-Entropy Moment Closures

More recently, a newer hierarchy of moment closures with many desirable properties was proposed. It is based on using the distribution function that maximizes the entropy while remains consistent with moments present in the solution vector, $\mathbf{U}$ [17, 23]. For classical gases, for which the entropy density is known to be $\langle \mathcal{F} \ln \mathcal{F} \rangle$ [21], and using the method of Lagrange multiplier, one can show that the assumed distribution function has a form of

$$\mathcal{F}\left(x_i, v_i, t\right) = e^{\boldsymbol{\alpha}^T M} . \tag{2.27}$$

As can be seen, the distribution function is positive valued, a property that Grad-type closure lacks, and stays finite for appropriately chosen velocity weights [17]. Also, it can be shown that the resulting moment equations are globally hyperbolic and well-posed. Beside these advantages, the maximum entropy distribution is also pleasing due to the fact that particle collisions are known to always cause the entropy to increase. Therefore, high-entropy distribution are usually the most likely. The lowest-order member of this hierarchy is a 5-moment closure, which leads to the familiar Euler equations. It is found by taking the generating weight to be $\mathbf{M} = [m, mv_i, mv_iv_i]^T$. The Gaussian closure is the second lowest-order closure derived from the maximum-entropy closure by taking $\mathbf{M} = [m, mc_i, mc_ic_j]^T$

weights. It consists of 10 moment equations and yield a strictly hyperbolic treatment for a compressible, viscous, adiabatic gas [17, 15, 20, 27].

Despite the mathematical and physical arguments presented here, maximum-entropy closures suffer from two major problems. Firstly, it has been found that for any moment systems that include third-order moments or higher-order moments, the coefficients of the distribution function, $\boldsymbol{\alpha}$, cannot be written in closed form. Since the simplest closure that offers a treatment for heat flux includes third-order moments, facing this problem is unavoidable. In order to overcome this problem, a very expensive, poorly conditioned iterative technique is needed to calculate the coefficients of the distribution function [19]. This expensive procedure must be carried out every time a flux is required during a numerical computation. Secondly, Junk has shown that there are physically possible moments for which the entropy-maximization problem, on which the whole theory is based, has no solution [13]. In these instances, the whole theory falls apart. More disastrousness still is the fact that local equilibrium always lies on the boundary of this subspace of ill-definition.

2.4.3 A Closed-Form Approximation to Maximum-Entropy

Recently, a new technique has been proposed to construct closed-form approximations to higher-order maximum-entropy moment closures [21]. The new technique is based on interpolation of closed-form expressions that follow the original maximum-entropy solution wherever the entropy-maximization problem can be solved explicitly, and interpolates with simple function otherwise. The technique is developed for both one- and three-dimensional gases. A one-dimensional gas is a gas that has its particle's location and velocity both defined by a scalar value. In order to permit the most detailed study of these new closures,

the one-dimensional system is considered in this work. More details of the derivation of the new technique for three-dimensional gases is given in [21].

The simplest closure of this type that offers a treatment for heat flux is a fourteen-moment closure, generated using the weight vector $\mathbf{M} = [m, mv_i, mv_iv_j, mv_iv_jv_j, mv_iv_iv_jv_j]^T$, for a three-dimensional system. However, for a one-dimensional case the weight vector simplifies to $\mathbf{M} = [m, mv, mv^2, mv^3, mv^4]^T$ by restricting both physical space, x_i, and velocity space, v_i, to be one-dimensional. The resulting system of five-moment equations using the BGK collision operator is

$$\frac{\partial \rho}{\partial t} + \frac{\partial}{\partial x}(\rho u) = 0\,, \tag{2.28}$$

$$\frac{\partial}{\partial t}(\rho u) + \frac{\partial}{\partial x}(\rho u^2 + p) = 0\,, \tag{2.29}$$

$$\frac{\partial}{\partial t}(\rho u^2 + p) + \frac{\partial}{\partial x}(\rho u^3 + 3up + q) = 0\,, \tag{2.30}$$

$$\frac{\partial}{\partial t}(\rho u^3 + 3up + q) + \frac{\partial}{\partial x}(\rho u^4 + 6u^2p + 4uq + r) = -\frac{q}{\tau}\,, \tag{2.31}$$

$$\frac{\partial}{\partial t}(\rho u^4 + 6u^2p + 4uq + r) + \frac{\partial}{\partial x}(\rho u^5 + 10u^3p + 10u^2q + 5ur + s) = -\frac{1}{\tau}\left(4uq + r - 3\frac{p^2}{\rho}\right)\,. \tag{2.32}$$

The moments present in the system are

$$\rho = \langle m\mathcal{F}\rangle\,, \quad \rho u = \langle mv\mathcal{F}\rangle\,,$$

$$p = \left\langle mc^2\mathcal{F}\right\rangle\,, \quad q = \left\langle mc^3\mathcal{F}\right\rangle\,,$$

$$r = \left\langle mc^4\mathcal{F}\right\rangle\,, \quad s = \left\langle mc^5\mathcal{F}\right\rangle\,,$$

where q is the heat flux, r and s are so called forth and fifth moments respectively. As can be clearly seen, the only moment that is used in the flux vector but is not present in the

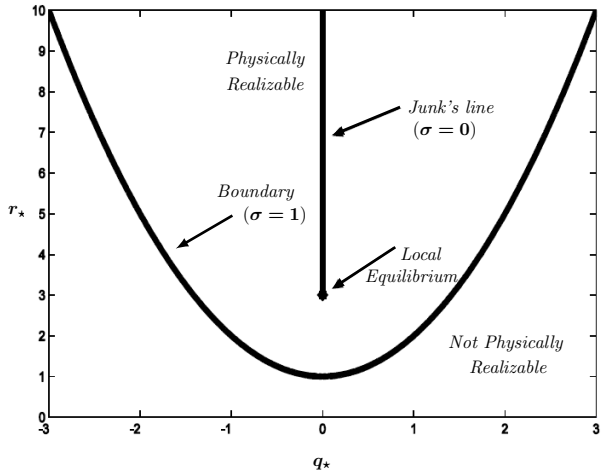

Figure 2.3: *Realizability region of the one-dimensional 5-moment system.*

solution vector is s. Therefore, to close the system, s must be expressed as a function of the first five moments. In order to do that, a new variable, σ, is defined as

$$\sigma\left(q_\star, r_\star\right) = \frac{3 - r_\star + \sqrt{(3 - r_\star) + 8q_\star^2}}{4}\,. \tag{2.33}$$

Stars denote non-dimensional moments, non-dimensionalized such that $\rho = 1$ and $p = 1$. This leads to non-dimensionalized third, fourth and fifth moments given by

$$q_\star = \frac{1}{\rho}\left(\frac{\rho}{p}\right)^{\frac{3}{2}} q, \qquad r_\star = \frac{1}{\rho}\left(\frac{\rho}{p}\right)^{2} r, \qquad s_\star = \frac{1}{\rho}\left(\frac{\rho}{p}\right)^{\frac{5}{2}} s.$$

Using these non-dimensional moments, it can be shown that there are restrictions on what moment states are physically possible [12]. Much like densities and pressure must be positive, it can be shown that only states for which $r_\star \geq q_\star^2 + 1$ are possible. Figure 2.3 shows a representation of realizable states for this system. Local equilibrium is at the point $q_\star = 0$ and $r_\star = 3$. Also, it can be seen that $\sigma = 0$ corresponds to states for which there is no maximum-entropy distribution function—the Junk subspace. The true maximum-entropy value of s cannot be found over most of this space. However, the

entropy-maximization problem can be solved in closed form both at local equilibrium and along the physical realizability limit. Based on these two solutions, an interpolation has been proposed [19, 21] as

$$s_\star = \frac{q_\star^3}{\sigma^2} + \left(10 - 8\sigma^{\frac{1}{2}}\right) q_\star \,. \tag{2.34}$$

This simple model, which approximates maximum-entropy, has proven to be robust and accurate for extreme non-equilibrium flows and maintains physical realizability. In order to validate the accuracy of this new model, a stationary shock problem was solved using the 5-moment closure [21]. Though many think of shock waves as discontinuous phenomena, if one looks on the scale of the mean free path one realizes that it is actually an abrupt yet continuous process. The abruptness of the transition typically causes a high degree of non-equilibrium behaviour. A comparison is made with results from this model, the Navier-Stokes equations and the BGK model, which can be regarded as the exact solution. As can be seen in Figure 2.4, results for the normalized density and non-dimensionalized heat flux as given by the five-moment closure stay close to BGK results while the Navier-Stokes results show significant deviations. As in the original maximum-entropy closure, the proposed approximation model also suffers from a singularity in the closing flux on Junk subspace (as $\sigma \to 0$). It has also been previously observed that the presence of this singularity in the closing flux leads to wavespeeds in the hyperbolic system that are arbitrarily large near the Junk line. The singular nature of the model has made more extensive numerical study of its capabilities difficult.

The objective of the present work is to develop a preconditioning technique for the five-moment system in order to deal with the singularity in the system and obtain finite fluxes

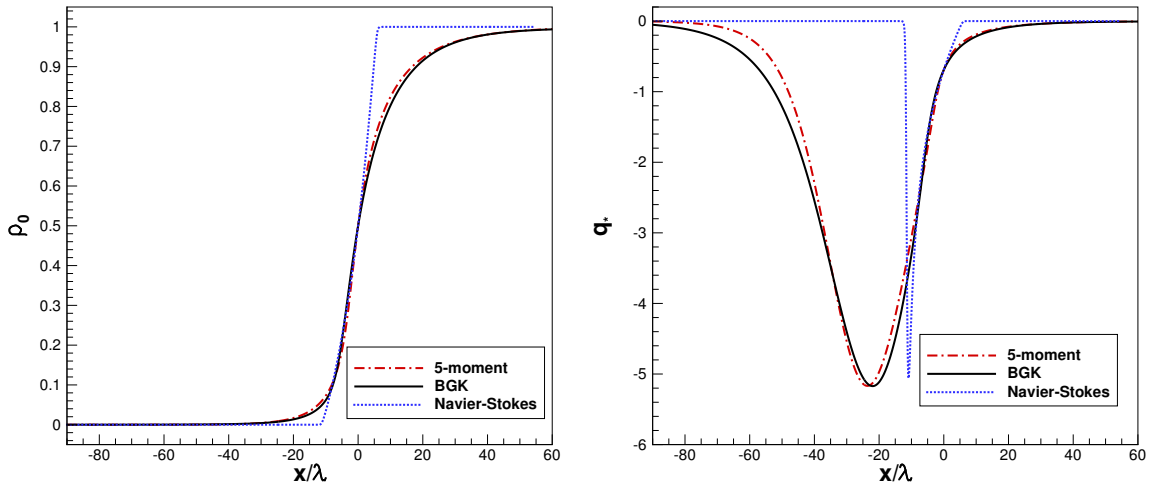

(a) *Normalized density* (b) *Non-dimensional heat flux*

Figure 2.4: *Mach-8 Shock Structure [21].*

and wavespeeds while maintaining the same solution quality as the non-preconditioned five-moment system.

Chapter 3

Analysis and Preconditioning of the 5-Moment System

As mentioned in the previous chapter, the goal of the current study is to adjust the 5-moment system in a way that the steady-state solution remains the same while removing the singularity from the equations and changing the wavespeeds such that they remain finite. In order to do this, one needs to study the mathematical behaviour of the 5-moment system, Equation (3.1), over the region of physically realizable states. For simplicity's sake, the five-moment equations is written in a vector form as

$$\frac{\partial \mathbf{U}}{\partial t} + \frac{\partial \mathbf{F}}{\partial x} = \mathbf{S}\,. \tag{3.1}$$

In Equation (3.1), $\mathbf{U}$ and $\mathbf{F}$ are the solution and flux vectors respectively and $\mathbf{S}$ is a vector denoting the collision operator's effect on the moments of the solution vector. As noted before, the BGK collision operator has been used throughout the current work. For the one-dimensional 5-moment system, the BGK operator, $\mathbf{S}$, is given by

$$\mathbf{S} = \left[0, 0, 0, -\frac{q}{\tau}, -\frac{1}{\tau}\left(4uq + r - 3\frac{p^2}{q}\right)\right]^T . \tag{3.2}$$

The solution and flux vectors can be written as [21],

$$\mathbf{U} = \begin{pmatrix} \rho \\ \rho u \\ \rho u^2 + p \\ \rho u^3 + 3up + q \\ \rho u^4 + 6u^2 p + 4uq + r \end{pmatrix}, \quad \mathbf{F} = \begin{pmatrix} \rho u \\ \rho u^2 + p \\ \rho u^3 + 3up + q \\ \rho u^4 + 6u^2 p + 4uq + r \\ \rho u^5 + 10u^3 p + 10u^2 q + 5ur + s \end{pmatrix}. \tag{3.3}$$

It can be clearly seen that the first entries in the solution and flux vectors are related such that

$$\mathbf{F}_i = \mathbf{U}_{i+1} \quad \text{for } i = 0, 1, 2, 3\,. \tag{3.4}$$

Here, i denotes the index of the entry in the vectors. This property will make analysis of the system's flux Jacobian much easier. Before a preconditioner for this system can be proposed, a thorough study of the eigenvalues of the flux Jacobian is required.

3.1 Eigenstructure of the 5-Moment System

It is well-known that the solutions of hyperbolic systems are characterized by waves. In order to understand the wave behaviour of this closed-form system, it is necessary to study the eigenstructure of its flux-Jacobian matrix, $\frac{\partial \mathbf{F}}{\partial \mathbf{U}}$. Due to the structure of the 5-moment closure, shown in Equation (3.4), this flux-Jacobian matrix takes the form of a companion

matrix, given as

$$\frac{\partial \mathbf{F}}{\partial \mathbf{U}} = \begin{bmatrix} 0 & 1 & 0 & 0 & 0 \\ 0 & 0 & 1 & 0 & 0 \\ 0 & 0 & 0 & 1 & 0 \\ 0 & 0 & 0 & 0 & 1 \\ a_0 & a_1 & a_2 & a_3 & a_4 \end{bmatrix} . \tag{3.5}$$

In order to restrict the range of states that must be studied in order to fully characterize the system, non-dimensional states are again considered. For a non-dimensional 5-moment system with zero bulk velocity, the entries in the last row of the Jacobian matrix can be written as a function of $q^\star$ and σ as

$$a_0 = \frac{2q_\star\left(\left(3-7\sigma+4\sigma^{1.5}\right)q_\star+6\sigma^{2.5}+4\sigma^{3.5}-10\sigma^3\right)}{\sigma(q_\star^2+2\sigma^2)} , \tag{3.6}$$

$$a_1 = \frac{(3-3\sigma)q_\star^4+\left(48\sigma^{2.5}-33\sigma^2-16\sigma^{3.5}\right)q_\star^2-30\sigma^4-20\sigma^5+48\sigma^{4.5}}{\sigma^2(q_\star^2+2\sigma^2)} , \tag{3.7}$$

$$a_2 = -\frac{2q_\star\left(\left(6-7\sigma+2\sigma^{1.5}\right)q_\star+12\sigma^{2.5}-10\sigma^3\right)}{\sigma(q_\star^2+2\sigma^2)} , \tag{3.8}$$

$$a_3 = -\frac{q_\star^4+\left(16\sigma^{2.5}-16\sigma^2\right){q^\star}^2-20\sigma^4+48\sigma^{4.5}}{\sigma^2(q_\star^2+2\sigma^2)} , \tag{3.9}$$

$$a_4 = \frac{2\left(q_\star^2\sqrt{\sigma}+2\sigma^3\right)q_\star}{\sigma^{1.5}(q_\star^2+2\sigma^2)} . \tag{3.10}$$

The eigenvalues of this Jacobian are the five wavespeeds of the system. In order to find the eigenvalues of this matrix, roots of the characteristic polynomial of the matrix are needed. As can be easily proven, a companion matrix has a characteristic equation of the form

$$\lambda^5 - a_4\lambda^4 - a_3\lambda^3 - a_2\lambda^2 - a_1\lambda^1 - a_0 = 0 . \tag{3.11}$$

It can be seen that the resulting polynomial is quintic. As such, the roots of the equation cannot be determined explicitly, this is due to the Abel-Ruffini theorem [7]. However, for situations in which one of the wavespeeds, or eigenvalues, is zero, the quintic polynomial degenerates to a quartic polynomial, which can be solved for its roots explicitly. As the ultimate goal here is to find approximations for the wavespeeds, the first step is to identify states for which one wavespeed is zero and find the exact value for the remaining four eigenvalues. These exact solutions can then be used as a guide to postulate effective approximations that span all admissible states.

3.1.1 Approximate Eigenvalues

In order to find states that have one zero eigenvalue, the behaviour of the wavespeeds is investigated numerically. This is simply done by numerically scanning the two-dimensional moment space that describes the non-dimensional system, as depicted in Figure 2.3. The investigation reveals that the 5-moment system has a zero wavespeed in three different situations. In these situations, the remaining four wavespeeds can be found analytically. These states are:

1. The first region is the line segment $q_\star = 0$ and $1 < r_\star < 3$. On this line, by symmetry, one eigenvalue must be zero. As $q_\star$ becomes zero, one can easily show that expressions (3.6) to (3.10) are equal to

$$a_0 = 0, \qquad a_1 = -10\sigma + 24\sqrt{\sigma} - 15, \qquad a_2 = 0, \qquad a_3 = 10 - 8\sqrt{\sigma}, \qquad a_4 = 0.$$

Therefore, if the characteristic equation given by the flux-Jacobian matrix is written again, it gives

$$\lambda^5 - a_3\lambda^3 - a_1\lambda^1 = 0\,. \tag{3.12}$$

Factoring λ, one obtains

$$\lambda\left(\lambda^4 - a_3\lambda^2 - a_1\right) = 0\,. \tag{3.13}$$

Equation (3.13) can be solved for its roots. The resulting roots are simply

$$\lambda_0 = -\lambda_4 = \sqrt{\frac{a_3+\sqrt{-a_3^2+4a_1}}{2}},$$

$$\lambda_2 = 0,$$

$$\lambda_1 = -\lambda_3 = \sqrt{\frac{a_3-\sqrt{-a_3^2+4a_1}}{2}}\,.$$

2. Another situation in which one of the wavespeeds is zero is on the boundary of the physically realizable region where $\sigma = 1$, and $r_\star = q_\star^2 + 1$.

   Substituting $\sigma = 1$ into the expressions (3.6) to (3.10) yields

$$a_0 = 0, \qquad a_1 = -1, \qquad a_2 = -2q_\star, \qquad a_3 = 2 - q_\star^2, \qquad a_4 = 2q_\star.$$

   The characteristic polynomial for states on this boundary is given by

$$\lambda^5 - 2q_\star\lambda^4 - \left(2 - q_\star^2\right)\lambda^3 + 2q_\star\lambda^2 + \lambda^1 = 0\,. \tag{3.14}$$

   Factoring λ, one obtains

$$\lambda\left(\lambda^4 - 2q_\star\lambda^3 - \left(2 - q_\star^2\right)\lambda^2 + 2q_\star\lambda^1 + 1\right) = 0\,. \tag{3.15}$$

The roots that satisfy Equation (3.15) are

$$\lambda_0 = \lambda_1 = \frac{q_\star + \sqrt{q_\star^2+4}}{2},$$

$$\lambda_2 = 0,$$

$$\lambda_3 = \lambda_4 = \frac{q_\star - \sqrt{q_\star^2+4}}{2}.$$

3. It has also been observed through numerical investigation that in the limit of $r_\star \to \infty$, one of the wavespeeds becomes zero. For the analysis at very large values of $r_\star$, it is more convenient to express the entries in the flux Jacobian in terms of $q_\star$, $r_\star$, $s_\star$, $\frac{\partial s_\star}{\partial r_\star}$, and $\frac{\partial s_\star}{\partial q_\star}$. Using these expressions, Equations (3.6) to (3.10) take the form

$$a_0 = \tfrac{1}{2}\left(-3s_\star + 2r_\star \tfrac{\partial s_\star}{\partial r_\star} + q_\star \tfrac{\partial s_\star}{\partial q_\star}\right), \tag{3.16}$$

$$a_1 = 5r_\star - 4q_\star \tfrac{\partial s_\star}{\partial r_\star} - 3\tfrac{\partial s_\star}{\partial q_\star}, \tag{3.17}$$

$$a_2 = \tfrac{1}{2}\left(5s_\star - 4r_\star \tfrac{\partial s_\star}{\partial r_\star} - 3q_\star \tfrac{\partial s_\star}{\partial q_\star}\right), \tag{3.18}$$

$$a_3 = \tfrac{\partial s_\star}{\partial q_\star}, \tag{3.19}$$

$$a_4 = \tfrac{\partial s_\star}{\partial r_\star}. \tag{3.20}$$

In order to make the derivation of the closing flux more convenient, $r_\star$ is written as a function of σ and $q_\star$

$$r_\star = \frac{q_\star^2}{\sigma} + 3 - 2\sigma \quad \text{for } 0 \le \sigma \le 1. \tag{3.21}$$

Since $(3-2\sigma)$ varies only between 1 and 3, very high values of $r_\star$ must mean that $\frac{q_\star^2}{\sigma}$ is dominating in Equation (3.21). Thus,

$$r_\star \approx \frac{q_\star^2}{\sigma}, \tag{3.22}$$

or

$$\sigma \approx \frac{q_\star^2}{r_\star}\,. \tag{3.23}$$

Using the same argument, one can approximate $s_\star$ as a function of $q_\star$ and $r_\star$ when $r_\star \to \infty$ such that

$$s_\star \approx \frac{r_\star^2}{q_\star}\,. \tag{3.24}$$

This leads to

$$\frac{\partial s_\star}{\partial r_\star} \approx \frac{2r_\star}{q_\star}\,, \tag{3.25}$$

$$\frac{\partial s_\star}{\partial q_\star} \approx -\frac{r_\star^2}{q_\star 2}\,, \tag{3.26}$$

for large values of $r_\star$. Substituting Equations (3.23) to (3.26) into Equations (3.16) to (3.20), one obtains

$$a_0 = 0, \qquad a_1 = 3\sigma(\frac{q_\star}{\sigma})^2\left(\frac{1}{\sigma} - 1\right), \qquad a_2 = 0, \qquad a_3 = -(\frac{q_\star}{\sigma})^2, \qquad a_4 = 2\frac{q_\star}{\sigma}.$$

The resulting roots of the quartic characteristic polynomial written in the limit of $r_\star \to \infty$ are

$$\lambda_0 = \frac{q_\star + \sqrt{q_\star^2 + 4\sigma q_\star\sqrt{3 - 3\sigma}}}{2\sigma}\,,$$

$$\lambda_1 = \frac{q_\star + \sqrt{q_\star^2 - 4\sigma q_\star\sqrt{3 - 3\sigma}}}{2\sigma}\,,$$

$$\lambda_2 = 0\,,$$

$$\lambda_3 = \frac{q_\star - \sqrt{q_\star^2 - 4\sigma q_\star\sqrt{3 - 3\sigma}}}{2\sigma}\,,$$

$$\lambda_4 = \frac{q_\star - \sqrt{q_\star^2 + 4\sigma q_\star\sqrt{3 - 3\sigma}}}{2\sigma}\,.$$

Knowing the exact expressions for the eigenvalues of the flux Jacobian at these states and not being able to solve for the eigenvalues explicitly in any other areas, one could suggest approximating the eigenvalues for the whole realizability region based on interpolations between these exact values. By inspection of the form of the expressions on the limits, a closed-form approximation for the exact eigenvalues throughout the domain is proposed. The proposed approximate eigenvalues are given by

$$\lambda_0 = \frac{q_\star + \sqrt{q_\star^2 - \frac{4}{5} q_\star \sigma C + 4\sigma^2 Y}}{2\sigma} + E\,, \tag{3.27}$$

$$\lambda_1 = \frac{q_\star + \sqrt{q_\star^2 - \frac{6}{5} q_\star \sigma C + 4\sigma^2 X}}{2\sigma} - D\,, \tag{3.28}$$

$$\lambda_2 = \frac{2\left(q_\star^2\sqrt{\sigma} + 2\sigma^3\right) q_\star}{\sigma^{1.5}(q_\star^2 + 2\sigma^2)} - \lambda_0 - \lambda_1 - \lambda_3 - \lambda_4\,, \tag{3.29}$$

$$\lambda_3 = \frac{q_\star - \sqrt{q_\star^2 + \frac{6}{5} q_\star \sigma C + 4\sigma^2 X}}{2\sigma} + D\,, \tag{3.30}$$

$$\lambda_4 = \frac{q_\star - \sqrt{q_\star^2 + \frac{4}{5} q_\star \sigma C + 4\sigma^2 Y}}{2\sigma} - E\,, \tag{3.31}$$

where

$$C = \sqrt{3 - 3\sigma}\,,$$

$$X = A + D^2 + 2\sqrt{A}D\,, \qquad Y = B + E^2 - 2\sqrt{B}E\,,$$

$$A = 5 - 4\sqrt{\sigma} - \sqrt{10 - 16\sqrt{\sigma} + 6\sigma}\,, \qquad B = 5 - 4\sqrt{\sigma} + \sqrt{10 - 16\sqrt{\sigma} + 6\sigma}\,,$$

$$D = \frac{3}{10}\sqrt{3 - 3\sigma}\,, \qquad E = \frac{8}{10}\sqrt{3 - 3\sigma}\,.$$

A comparison is made between the approximate eigenvalues given by Equations (3.27) to (3.31) and the numerically computed exact eigenvalues of the 5-moment system and is shown in Figure 3.1 for several values of σ. It is clear to see that the approximate eigenvalues stay very close to the exact ones through the different range of σ and $q_\star$. For σ

equal to 1, only three distinct wavespeeds exist, as is expected from numerical experience. However, for $0 < \sigma < 1$, five distinct wavespeeds are present and the proposed expressions approximate the true values well.

3.1.2 Analysis of the Singularity in the Moment System

As mentioned before, it has been numerically observed that the closing flux of the 5-moment closure becomes arbitrarily large when the Junk subspace is approached, $\sigma \to 0$. Studying the behaviour of the approximate wavespeeds also shows that the absolute values of two of the approximate wavespeeds become arbitrarily large close to that line. Which two waves become singular depends on the sign of $q_\star$. As can be seen in Figure 3.2, for small values of σ and positive $q_\star$, λ_0 and λ_1 in Equations (3.27) and (3.28) become extremely large while for negative $q_\star$, the same behaviour can be observed for λ_3 and λ_4. It is also observed that λ_2 always stays finite for any values of σ, therefore, it is not plotted here.

Since, by approaching to the Junk subspace, both σ and $q_\star$ approaches to zero, one could suggest rewriting the approximate-wavespeed equations in term of σ and $r_\star$ in order to isolate the dependence of the wavespeeds on only one vanishing parameter close to the Junk subspace. This could help to understand the exact behaviour of theses wavespeeds as they become arbitrarily large. Since we have

$$r_\star = \frac{q_\star^2}{\sigma} + 3 - 2\sigma \,, \tag{3.32}$$

one can rewrite Equation (3.32) as

$$q_\star = \pm\sqrt{\sigma\left(r_\star - 3 + 2\sigma\right)} \,. \tag{3.33}$$

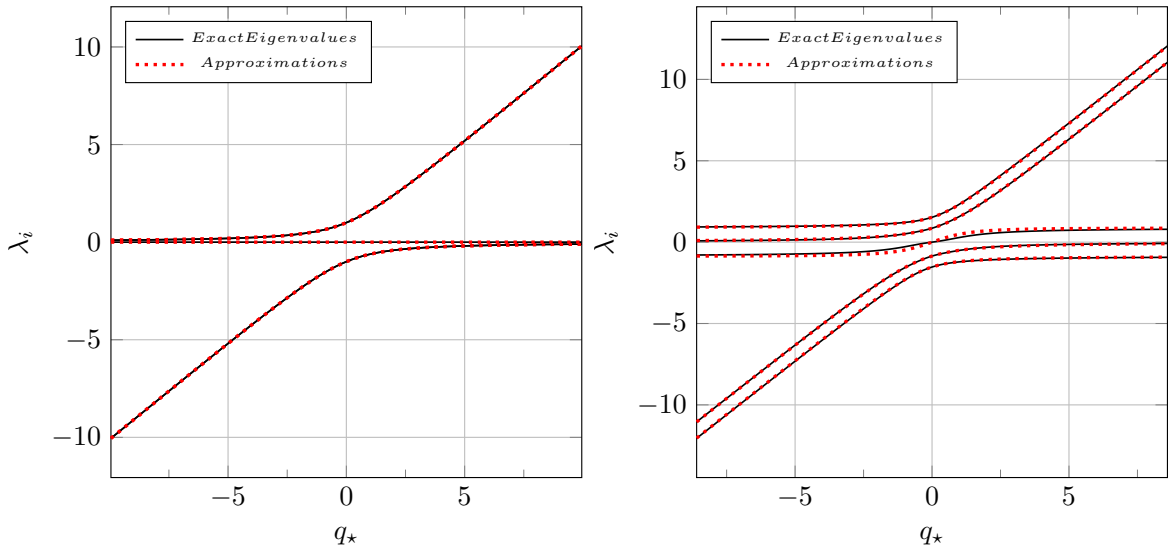

(a) $\sigma = 1$ (b) $\sigma = \frac{3}{4}$

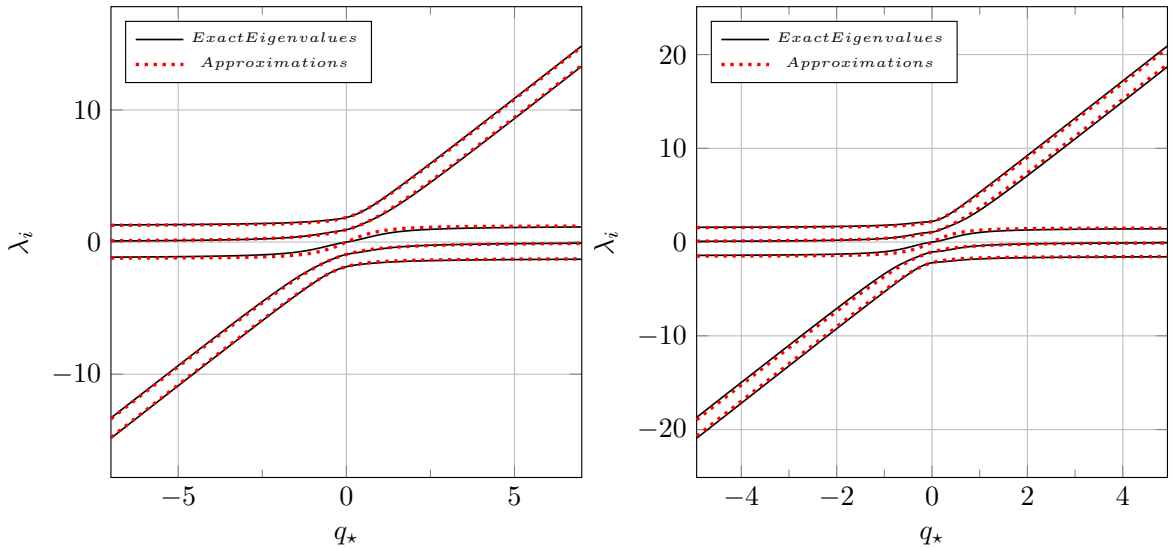

(c) $\sigma = \frac{1}{2}$ (d) $\sigma = \frac{1}{4}$

Figure 3.1: *Comparison of the exact eigenvalues of the 5-moment closure to the proposed approximations.*

Substituting this into λ_0 and λ_1 in Equations (3.27) and (3.28) when $q_\star$ is positive results in

$$\lambda_0 = \frac{\sqrt{r_\star - 3 + 2\sigma} + \sqrt{(r_\star - 3 + 2\sigma) - \frac{4}{5}\sqrt{\sigma(r_\star - 3 + 2\sigma)}C + 4\sigma Y}}{2\sqrt{\sigma}} + E\,, \tag{3.34}$$

$$\lambda_1 = \frac{\sqrt{r_\star - 3 + 2\sigma} + \sqrt{(r_\star - 3 + 2\sigma) - \frac{6}{5}\sqrt{\sigma(r_\star - 3 + 2\sigma)}C + 4\sigma Y}}{2\sqrt{\sigma}} - D\,. \tag{3.35}$$

Since the numerator of both equations are positive when σ goes to zero, it can be seen that the wavespeeds go to infinity at a rate of $\frac{1}{\sqrt{\sigma}}$. Using the same argument, one can show that for negative value of $q_\star$, λ_3 and λ_4 become infinite similarly as σ goes to zero.

$$\lambda_3 = \frac{-\sqrt{r_\star - 3 + 2\sigma} - \sqrt{(r_\star - 3 + 2\sigma) + \frac{6}{5}\sqrt{\sigma(r_\star - 3 + 2\sigma)}C + 4\sigma Y}}{2\sqrt{\sigma}} + D \tag{3.36}$$

$$\lambda_4 = \frac{-\sqrt{r_\star - 3 + 2\sigma} - \sqrt{(r_\star - 3 + 2\sigma) + \frac{4}{5}\sqrt{\sigma(r_\star - 3 + 2\sigma)}C + 4\sigma Y}}{2\sqrt{\sigma}} - E \tag{3.37}$$

As mentioned before, having infinitely large fluxes and wavespeeds in the system causes problems in numerical computation. These are two obvious problems that make numerical computation difficult. First, it is simply impossible to represent arbitrarily large numbers using finite-precision arithmetic—numerical overflows would be unavoidable. Second, very high wavespeeds will cause the problem to become numerically stiff, steady-state solutions will be very difficult to obtain if an explicit time-marching method is used. This is because the stable time step that can be taken is limited by the fastest wavespeed and will tend to zero as the wavespeed gets large. To deal with this problem, one could suggest to find a way to change the wavespeeds of the proposed 5-moment system somehow such that the resulting wavespeeds stay finite for any value of σ. This should be done in such a way that the final computed solution is not altered. Therefore, it is suggested in the current study that, using the information gained in this eigenstructure analysis, a local-preconditioning

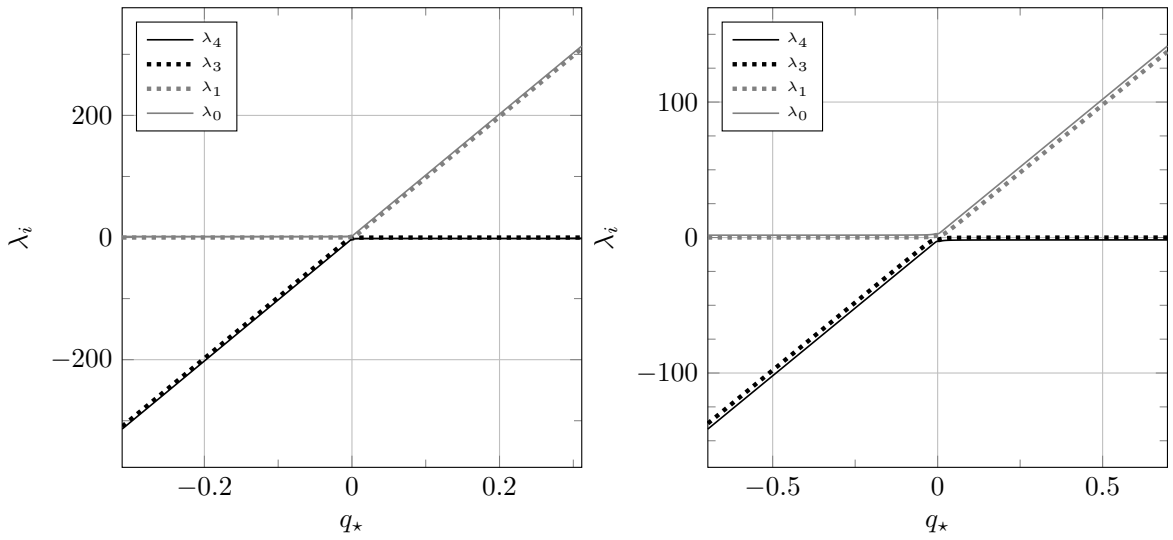

(a) $\sigma = 0.001$ (b) $\sigma = 0.005$

Figure 3.2: *Approximate eigenvalues of the 5-moment closure close to the Junk subspace*

technique for the 5-moment system is developed so that the wavespeeds remain finite throughout the physically realizable region.

3.2 Preconditioning

Preconditioning methods have been developed for a number of applications, including the aim of solving nearly incompressible flow problems using numerical algorithms designed for compressible flows [31, 32]. Chorin's [5] method of artificial compressibility for the incompressible Euler equations may be regarded as the oldest contribution to the field. More recently, a technique of preconditioning was suggested for the Navier-Stokes equations by Godfrey and Walters [8]. In these studies, the goal of preconditioning was to change the eigenvalues of the system of compressible flow equations in order to remove the large disparity of wavespeeds [31], which could cause stiffness in solving steady-state problems using a time-marching method. However, in the current study, the goal of preconditioning is

not necessarily to change the disparity of wavespeeds, as it has been used for incompressible/compressible flows, but to slow down the large wavespeeds of the 5-moment closure system around the Junk subspace and remove any possibility of numeric overflow during a practical computation.

3.2.1 Preconditioning of the 5-Moment System

The goal of the present study is to remove the possibility of singular fluxes or wavespeeds without altering the steady-state solution of the system. One possible technique is to pre-multiply both the space derivative and source terms in Equation (3.1) by a non-singular matrix. The preconditioned moment system can then be written as

$$\frac{\partial \mathbf{U}}{\partial t} + \mathbf{P}\frac{\partial \mathbf{F}}{\partial x} = \mathbf{PS}\,, \tag{3.38}$$

or

$$\frac{\partial \mathbf{U}}{\partial t} + \mathbf{P}\frac{\partial \mathbf{F}}{\partial \mathbf{U}}\frac{\partial \mathbf{U}}{\partial x} = \mathbf{PS}\,, \tag{3.39}$$

where $\mathbf{P}$ is the non-singular preconditioning matrix. The preconditioned system, Equation (3.38), shares the same solution with the original 5-moment system at steady state, when the time derivative is zero. Despite having the same solution at steady state, the behaviour in time of the hyperbolic system in Equation (3.39) is different from that of the original non-preconditioned PDEs. The wavespeeds of the system now depend on the eigenvalues of the matrix $\mathbf{P}\frac{\partial \mathbf{F}}{\partial \mathbf{U}}$ rather than just $\frac{\partial \mathbf{F}}{\partial \mathbf{U}}$. The goal is to find a $\mathbf{P}$ such that the highest eigenvalues of $\frac{\partial \mathbf{F}}{\partial \mathbf{U}}$ are reduced.

Due to the interesting structure of a companion matrix, it is suggested to use a local preconditioner matrix such that the matrix obtained by multiplying the local preconditioner

and flux Jacobian, $\mathbf{P}\frac{\partial \mathbf{F}}{\partial \mathbf{U}}$, maintains the structure of a companion matrix. This limits the form of the preconditioner to be

$$\mathbf{P} = \begin{bmatrix} 1 & 0 & 0 & 0 & 0 \\ 0 & 1 & 0 & 0 & 0 \\ 0 & 0 & 1 & 0 & 0 \\ 0 & 0 & 0 & 1 & 0 \\ \phi_0 & \phi_1 & \phi_2 & \phi_3 & \phi_4 \end{bmatrix}, \tag{3.40}$$

so that

$$\mathbf{P}\frac{\partial \mathbf{F}}{\partial \mathbf{U}} = \begin{bmatrix} 0 & 1 & 0 & 0 & 0 \\ 0 & 0 & 1 & 0 & 0 \\ 0 & 0 & 0 & 1 & 0 \\ 0 & 0 & 0 & 0 & 1 \\ b_0 & b_1 & b_2 & b_3 & b_4 \end{bmatrix}. \tag{3.41}$$

Besides the advantage of dealing with a companion matrix, using a preconditioner in the form shown above also guarantees that all but the last equation are guaranteed to remain in a conservative form, as in the original 5-moment system. This is because the preconditoner only modifies the last equation in the system. This last equation contains the singular closing flux. Also in numerical computation, dealing with a sparse matrix could reduce the cost of the computation significantly.

That being said, the local preconditioner needs to be chosen such that the wavespeeds of the new system remains finite for all the states of the realizability region. That must

be done by choosing entries for the last row of the local-preconditioner matrix such that it exactly cancels the infinity in the eigenvalues of the flux Jacobian, $\frac{\partial \mathbf{F}}{\partial \mathbf{U}}$.

3.2.2 Proposed Local Preconditioner

As mentioned, through careful investigation of the approximate wavespeeds shown in the previous section, it is found that the eigenvalues that go to infinity do so at a rate of $\lambda_i \propto \frac{1}{\sqrt{\sigma}}$. Therefore, one could suggest multiplying each of the original wavespeeds by a function that cancel the $\frac{1}{\sqrt{\sigma}}$. It has been found that, if each wavespeed is multiplied by

$$W = \sqrt{\frac{\sigma}{r_\star - 3 + 3\sigma}}, \tag{3.42}$$

the resulting wavespeeds stay finite over the realizability region. This factor is carefully designed such that it cancels the $\frac{1}{\sqrt{\sigma}}$ singularity as the Junk line is approached, without preconditioning states below equilibrium on Figure 2.3, where the original model is well behaved.

In order to find a local preconditioner matrix, $\mathbf{P}$, that results in the multiplication of the eigenvalues of the original system by the factor W, it helps to review a property of all companion matrices. For an arbitrary companion matrix, such as the one given by the flux Jacobian, one can show that

$$a_0 = \lambda_0\lambda_1\lambda_2\lambda_3\lambda_4 \tag{3.43}$$

$$a_1 = -\left[\lambda_0\lambda_1\lambda_2\lambda_3 + \lambda_0\lambda_1\lambda_2\lambda_4 + \lambda_0\lambda_1\lambda_3\lambda_4 + \lambda_0\lambda_2\lambda_3\lambda_4 + \lambda_1\lambda_2\lambda_3\lambda_4\right] \tag{3.44}$$

$$a_2 = \lambda_0\lambda_1\lambda_2 + \lambda_0\lambda_1\lambda_3 + \lambda_0\lambda_1\lambda_4 + \lambda_0\lambda_2\lambda_3 + \lambda_0\lambda_2\lambda_4 + \lambda_0\lambda_3\lambda_4 + \lambda_1\lambda_2\lambda_3 + \lambda_1\lambda_2\lambda_4 + \lambda_2\lambda_3\lambda_4 \tag{3.45}$$

$$a_3 = -\left[\lambda_0\lambda_1 + \lambda_0\lambda_2 + \lambda_0\lambda_3 + \lambda_0\lambda_4 + \lambda_1\lambda_2 + \lambda_1\lambda_3 + \lambda_1\lambda_4 + \lambda_2\lambda_3 + \lambda_2\lambda_4 + \lambda_3\lambda_4\right] \tag{3.46}$$

$$a_4 = \lambda_0 + \lambda_1 + \lambda_2 + \lambda_3 + \lambda_4\,. \tag{3.47}$$

This property follows directly from Equation (3.11) and suggests that if each entry in the last row of the flux-Jacobian matrix is multiplied by W^n, where n denotes the number of wavespeeds that are multiplied with each other to form the entry, the resulting matrix will have eigenvalues equal to $W\lambda_i$. In another words, if one assumes the preconditioned system has eigenvalues, β_i, such that

$$\beta_i = W\lambda_i \quad \text{for } i = 0, 1, 2, 3 \text{ and } 4\,, \tag{3.48}$$

the corresponding companion matrix with those eigenvalues, based on Equations (3.43) to (3.47), is

$$\mathbf{P}\frac{\partial \mathbf{F}}{\partial \mathbf{U}} = \begin{bmatrix} 0 & 1 & 0 & 0 & 0 \\ 0 & 0 & 1 & 0 & 0 \\ 0 & 0 & 0 & 1 & 0 \\ 0 & 0 & 0 & 0 & 1 \\ W^5a_0 & W^4a_1 & W^3a_2 & W^2a_3 & Wa_4 \end{bmatrix}, \tag{3.49}$$

where the a's are the same as those given in the original flux-Jacobian matrix. One can easily verify that the roots of the characteristic polynomial of the matrix $\mathbf{P}\frac{\partial \mathbf{F}}{\partial \mathbf{U}}$ are the same

as those in Equation (3.48). The characteristic equation has the form

$$\beta^5 - Wa_4\beta^4 - W^2a_3\beta^3 - W^3a_2\beta^2 - W^4a_1\beta^1 - W^5a_0 = 0\,. \tag{3.50}$$

Dividing Equation (3.50) by W^5, one gets

$$(\frac{\beta}{W})^5 - a_4(\frac{\beta}{W})^4 - a_3(\frac{\beta}{W})^3 - a_2(\frac{\beta}{W})^2 - a_1(\frac{\beta}{W})^1 - a_0 = 0\,. \tag{3.51}$$

Substituting λ for $(\frac{\beta}{W})$, the Equation becomes

$$\lambda^5 - a_4\lambda^4 - a_3\lambda^3 - a_2\lambda^2 - a_1\lambda^1 - a_0 = 0\,, \tag{3.52}$$

which is the same characteristic equation of the original flux-Jacobian matrix in Equation (3.11). In other word

$$\lambda_i = \frac{\beta_i}{W}\,, \tag{3.53}$$

or

$$\beta_i = W\lambda_i\,. \tag{3.54}$$

Solving for the entries in $\mathbf{P}$ from Equation (3.40) is than a simple matter of linear algebra. The solution is

$$\phi_0 = a_1\left(W^4 - W^5\right)\,, \tag{3.55}$$

$$\phi_1 = a_2\left(W^3 - W^5\right)\,, \tag{3.56}$$

$$\phi_2 = a_3\left(W^2 - W^5\right)\,, \tag{3.57}$$

$$\phi_3 = a_4\left(W^1 - W^5\right)\,, \tag{3.58}$$

$$\phi_4 = W^5\,, \tag{3.59}$$

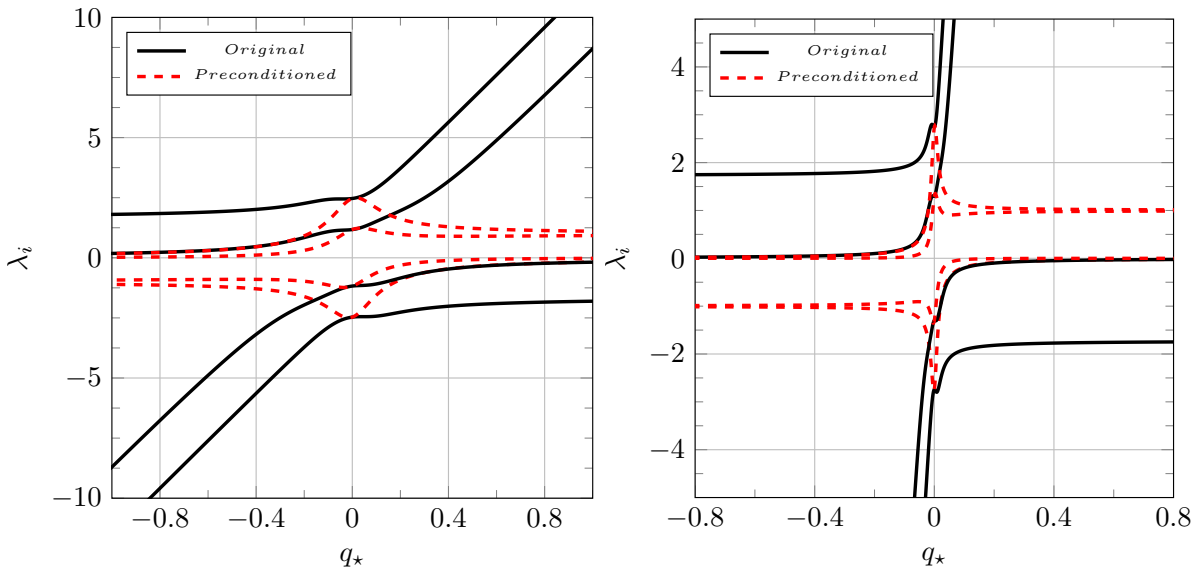

(a) $\sigma = 0.1$ (b) $\sigma = 0.01$

Figure 3.3: *Comparison of eigenvalues of the original and preconditioned 5-moment closure.*

with the a_i given in Equations (3.6) to (3.10) and W given by Equation (3.42). As all the original wavespeeds are simply scaled by a positive number, the preconditioned system remains hyperbolic over the realizability region, however, as mentioned before, the final equation is no longer expressible in conservation form. A comparison is made between the two systems for small values of σ in Figure 3.3. It can be seen that the wavespeeds of the proposed preconditioned system remain finite even for very small values of σ, where the original 5-moment system's wavespeeds diverge to infinity.

Figure 3.3 also confirms that, with decreasing σ, the eigenvalues of the original non-preconditioned 5-moment closure approach infinity with a steeper slope. The natural logarithm of the biggest wavespeed of the original and preconditioned systems over a large range of physically realizable states is plotted in Figure 3.4 for two non-dimensional reference velocities, $u_\star$. As can be seen, for the original 5-moment system, the maximum wavespeed becomes extremely large as the Junk line is approached, however, for the pre-

conditioned 5-moment system, the biggest wavespeed remains of the same order over the entire domain. It is also demonstrated that, for the reference velocity equal to zero, the maximum wavespeed is a symmetric function of $q_\star$, which is expected.

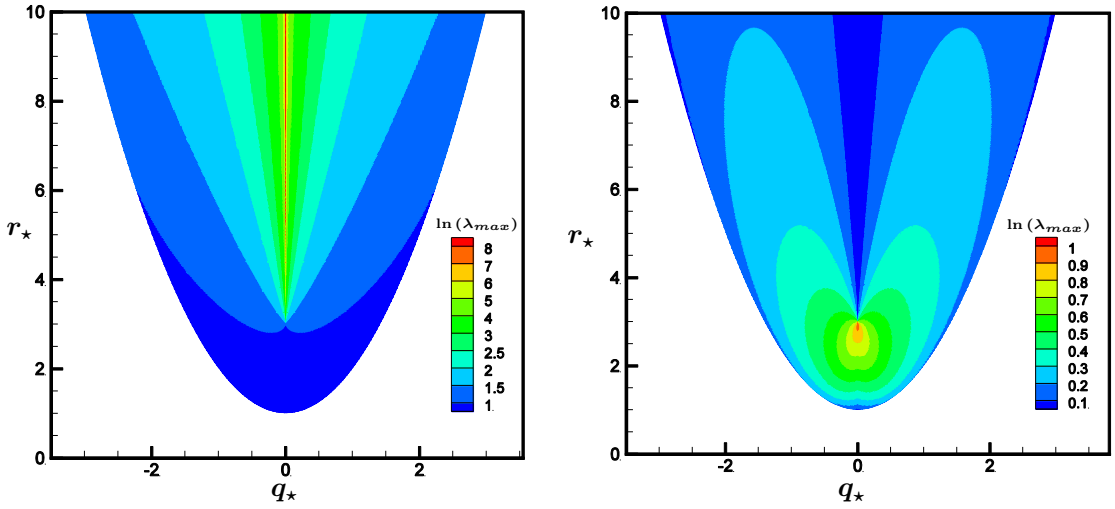

(a) *Original system,* $u^\star = 0$ (b) *Preconditioned system,* $u^\star = 0$

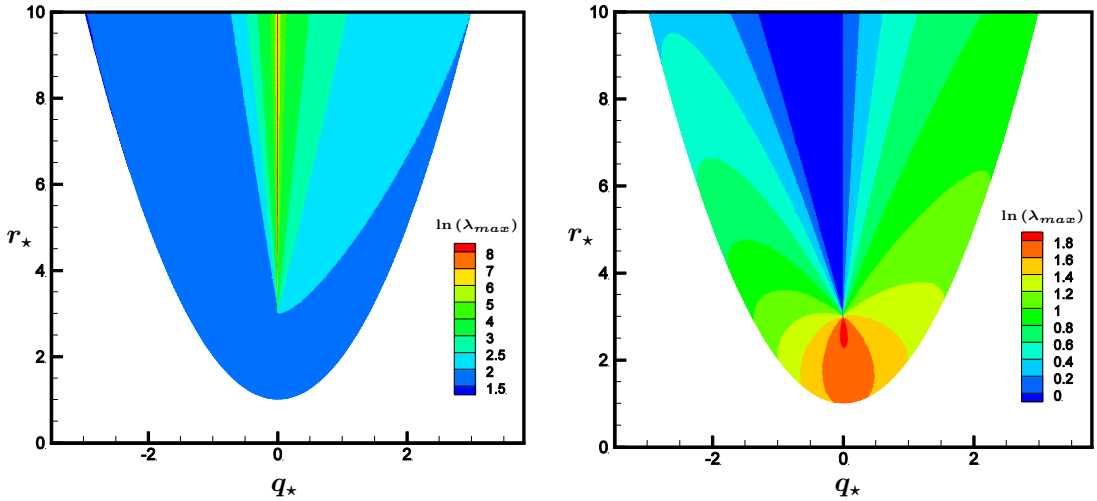

(c) *Original system,* $u^\star = 4$ (d) *Preconditioned system,* $u^\star = 4$

Figure 3.4: *Comparison of the natural logarithm of the maximum eigenvalues of the original and preconditioned 5-moment closure over the realizability zone (a)–(b)* $u^\star = 0$*; (c)–(d)* $u^\star = 4$.

Chapter 4

Numerical Method

The governing partial differential equations outlined in the previous chapter provide the time-evolution description of macroscopic quantities of a compressible gas in the continuum and transient regimes. This chapter presents the details of the proposed method developed for the numerical computation of the solution of these equations. Section 4.1 summarizes the development of a centred-finite-difference scheme used for solving the hyperbolic partial differential equations. It is based on the classical Lax-Friedrichs scheme [16]. Section 4.2 describes the implementation of a dual time-stepping extension to the centred finite-difference scheme in order to guarantee that the preconditioned system follows an evolution that is similar to the path that the unmodified 5-moment closure would follow. This was found to be required to ensure that the solutions remain in the range of physically possible states and for problems to remain well-posed. In Section 4.3, a brief review is given of explicit and implicit time-marching schemes and the resulted system of partial differential equations in the previous section is discretized in time.

4.1 Centred Finite-Difference Method

The finite-difference method used in the current study is based on the classical Lax-Friendrichs scheme. Since the proposed preconditioned system in Equation (3.39) can only be written in non-conservative form, the usual techniques involving approximate Riemann solvers (HLLE, Roe, etc) cannot be used. As a result, a centred scheme is used by adding artificial dissipation in order to produce a stable method.

4.1.1 Lax-Friedrichs Scheme

The Lax-Friedrichs scheme is a numerical method for the solution of hyperbolic partial differential equations that are expressed in conservation form. It can be viewed as a finite-difference method and is an alternative to Godunov's method (a very common finite-volume scheme for hyperbolic conservation laws) [9]. In this method, a stable solution for the hyperbolic PDEs is obtained by explicitly adding artificial viscosity to stabilize the calculation. This is in contrast to Godunov-type schemes, where the approximate solution of Riemann problems automatically adds the dissipation required for stability.

The traditional Lax-Friedrichs scheme can be used to solve one-dimensional non-linear hyperbolic PDEs of the form,

$$\frac{\partial \mathbf{U}}{\partial t} + \frac{\partial \mathbf{F}}{\partial x} = 0\,. \tag{4.1}$$

Here, $\mathbf{U}$ is the conservative solution vector and $\mathbf{F}$ is the flux vector. The Lax-Friedrichs discrete version of Equation (4.1) is

$$\mathbf{U}_i^{n+1} = \mathbf{U}_i^n - \frac{\Delta t}{2\Delta x}\left[\mathbf{F}_{i+1}^n - \mathbf{F}_{i-1}^n\right] + \frac{1}{2}\left[\mathbf{U}_{i+1}^n - 2\mathbf{U}_i^n + \mathbf{U}_{i-1}^n\right]\,. \tag{4.2}$$

Here, n denotes the time index of the time-marching scheme and i shows the cell number in a uniform one-dimensional grid. The last term in the right-hand side of the equation is known as the artificial dissipation as it approximates the second derivation of a diffusion operator. Without the addition of the dissipation term in Equation (4.2), one ends up with the forward-time centred-space scheme, which is unconditionally unstable for hyperbolic problems. Since the standard Lax-Friedrichs method only applies to conservative hyperbolic PDEs, an adjustment to the scheme is needed in order to use it for a non-conservative system such as the one resulting from the preconditioned 5-moment closure in the previous chapter.

4.1.2 Proposed Centred-Difference Scheme

As mentioned before, due to the preconditioning of the 5-moment closure, the system can no longer be written in conservation form. Traditional methods for the solution of hyperbolic conservation laws rely on the equations being expressible in conservation form, and are thus inapplicable. The development of numerical methods for the solution of non-conservative hyperbolic equations is still a very active area of research [28, 3, 24]. For the current research, a modified form of the Lax-Friedrichs scheme is used. Though this scheme is only first-order accurate, it will be sufficient to evaluate the effectiveness of the preconditioner. The derivation begins with the preconditioned system of PDEs,

$$\frac{\partial \mathbf{U}}{\partial t} + \mathbf{P}\frac{\partial \mathbf{F}}{\partial \mathbf{U}}\frac{\partial \mathbf{U}}{\partial x} = \mathbf{PS}\,. \tag{4.3}$$

Defining $\mathbf{A} = \mathbf{P}\frac{\partial \mathbf{F}}{\partial \mathbf{U}}$, one can rewrite Equation (4.3) as

$$\frac{\partial \mathbf{U}}{\partial t} + \mathbf{A}\frac{\partial \mathbf{U}}{\partial x} = \mathbf{PS}\,. \tag{4.4}$$

The procedure used to advance cell i from time index n to time index $n+1$ is given by the equation

$$\mathbf{U}_i^{n+1} = \mathbf{U}_i^n - \frac{\Delta t}{2\Delta x}\mathbf{A}_i^n\left[\mathbf{U}_{i+1}^n - \mathbf{U}_{i-1}^n\right] + \frac{\Delta t}{2\Delta x}\mathbf{P}_i^n\left[\mathbf{U}_{i+1}^n - 2\mathbf{U}_i^n + \mathbf{U}_{i-1}^n\right] + \Delta t\mathbf{P}_i^n\mathbf{S}_i^n\,. \tag{4.5}$$

This treatment uses explicit-Euler time marching, a centred-difference approximation to the term involving the first derivative in space and contains an added artificial dissipation term for stability. It can be seen that this term is a finite-difference approximation of $\frac{\Delta x}{2}\frac{\partial^2 \mathbf{U}}{\partial x^2}$, thus it is a dissipation term that will vanish as $\Delta x \to 0$.

Though this scheme is stable, it was found that it often could not be used to solve the preconditioned system. This is because, even though this preconditioned system shares the same steady-state solution as the original system, the path taken in time is altered. It was found that the time evolution of most initial value problems took the system outside the region of physically realizable states. Outside this region, the system become ill-posed and computations cannot continue. In order to avoid this, it is required to adjust the finite-difference scheme in a way that allow the simulations to follow almost the same path as the original 5-moment closure towards the steady-state solution. This is done using a dual-time-stepping strategy.

4.2 Dual Time Stepping

Initially, it may seem like a bad trade to gain finite fluxes and wavespeeds only to appear to lose well-posedness. Ideally, one could use the preconditioner to remove the system singularities without altering the evolution of the original seemingly well-posed system. This can actually be accomplished by using a technique known as a dual time stepping. Additionally, by applying a dual time-stepping scheme to the preconditioned system, time accuracy can also be regained. The resulting scheme is therefore applicable to unsteady problems. In this technique, the flow field is advanced through an inner pseudo-time loop where preconditioning is applied. Each time that this inner loop is advanced to steady-state, the system is advanced in a time-accurate way to the next time step in an outer loop that represents real physical time.

The new modified system of PDEs, with additional pseudo time, can be written as

$$\frac{\partial \mathbf{U}}{\partial \tau} + \mathbf{P}\frac{\partial \mathbf{U}}{\partial t} + \mathbf{A}\frac{\partial \mathbf{U}}{\partial x} = \mathbf{PS}\,, \tag{4.6}$$

where t indicate the physical time. Here, τ is used to demonstrate pseudo-time. This is not directly related to the relaxation time in Equation (2.19). No confusion should result from the reuse of the symbol. The first term in the left-hand side of the Equation (4.6), $\frac{\partial \mathbf{U}}{\partial \tau}$, has been used to show the time derivative of the vector $\mathbf{U}$ with respect to pseudo time, whereas $\frac{\partial \mathbf{U}}{\partial t}$ is the time derivative of $\mathbf{U}$ with respect to physical time. It can be easily seen that, as the solution converges to a steady state in pseudo time, $\frac{\partial \mathbf{U}}{\partial \tau} \approx 0$, Equation (4.6) becomes

$$\mathbf{P}\frac{\partial \mathbf{U}}{\partial t} + \mathbf{A}\frac{\partial \mathbf{U}}{\partial x} = \mathbf{PS} \tag{4.7}$$

knowing $\mathbf{A} = \mathbf{P}\frac{\partial \mathbf{F}}{\partial \mathbf{U}}$, one can rewrite Equation (4.7) as

$$\frac{\partial \mathbf{U}}{\partial t} + \frac{\partial \mathbf{F}}{\partial \mathbf{U}}\frac{\partial \mathbf{U}}{\partial x} = \mathbf{S} \tag{4.8}$$

which is exactly the same equation as the one given by the original 5-moment closure. The exact way in which a problem can be advanced in a fictitious pseudo time to points in real time becomes evident when a discretized version of Equation (4.6) is considered,

$$\begin{aligned}\mathbf{U}_i^{n+1} = \mathbf{U}_i^n - \tfrac{\Delta\tau}{\Delta t}\mathbf{P}_i^n\left[\mathbf{U}_i^n - \mathbf{U}_i^m\right] - \tfrac{\Delta\tau}{2\Delta x}\mathbf{A}_i^n\left[\mathbf{U}_{i+1}^n - \mathbf{U}_{i-1}^n\right] \quad . \\ + \tfrac{\Delta\tau}{2\Delta x}\mathbf{P}_i^n\left[\mathbf{U}_{i+1}^n - 2\mathbf{U}_i^n + \mathbf{U}_{i-1}^n\right] + \Delta\tau\mathbf{P}_i^n\mathbf{S}_i^n\end{aligned} \tag{4.9}$$

where n and m denote the time index in pseudo time and physical time respectively. It is now clear how one can advance the preconditioned system between multiple "steady states" in pseudo time, each of which corresponds to time instances of a time-accurate calculation in real time. At the beginning of a time step in physical time from index "m" to "$m+1$", $\mathbf{U}^n$ will equal $\mathbf{U}^m$. As the system is advanced in pseudo time, $\mathbf{U}^n$ is advanced to $\mathbf{U}^{n+1}$, $\mathbf{U}^{n+2}$, and so forth while $\mathbf{U}^m$ is held fixed. At steady state in pseudo time, $\mathbf{U}^n = \mathbf{U}^{n+1}$, what remains in Equation (4.9) is a discrete representation of Equation (4.8), the non-preconditioned model. At this point, looking at the second term on the right-hand side of Equation (4.9), it is clear that $\mathbf{U}^n$ is now equal to $\mathbf{U}^{m+1}$. Moreover, since, in the last iteration in pseudo time, all the other terms were evaluated at state $\mathbf{U}^n$, they also all correspond to state $\mathbf{U}^{m+1}$—the next time instance in physical time. The two time marching schemes are therefore: explicit Euler in pseudo time and implicit Euler in physical time.

4.3 Explicit vs Implicit Time-Marching Models

Explicit time-marching methods are widely used for solving steady-state problems in computational fluid dynamics. They are popular because they tend to be easy to implement and code using this technique can be used to efficiently solve both time-accurate and steady problems. Explicit methods use the state of the system at the current time in order to calculate an update to find the state of the system at a later time. Unfortunately, explicit methods tend to have restrictions on the maximum stable time step that can safely be taken—progress to steady state is limited by this restriction. For problems where physical effects occur on different time scales (stiff problems), convergence to steady state can be very slow. When time-accurate information is not important, such as in the inner pseudo-time loop, they tend to be a poor choice.

4.3.1 Implicit Schemes

Implicit time-marching schemes offer a possibly improved method for solving numerically stiff equations such as the one in Equation (4.6). Since these type of schemes are less sensitive to the stiffness of the system and they are not as restricted by the usual stability conditions. As a result, it can be possible to take arbitrarily big time steps and move to steady state very rapidly. Implicit schemes are so named because the update from time index n to $n+1$ is "evaluated" at index $n+1$. To accomplish this, a large system of coupled equations must be solved for each step in time. However, for numerically stiff problems, an implicit scheme could allow a sufficiently large time step to be taken such that it offsets the more expensive computational cost per iteration and results in faster convergence to

solution.

Various types of implicit time-marching schemes have been developed for solving partial differential equations. In the current study, the implicit Euler scheme is used to discretize the non-linear ordinary differential equations resulting from the spacial discretization in pseudo time. For simplicity's sake, a new set of variables is introduced. Using these variables, one can rewrite the original explicit method described in Equation (4.9) in the following form:

$$\frac{1}{\Delta\tau}\Delta\mathbf{U}_i = \mathbf{B}_i^n + \mathbf{C}_i^n + \mathbf{D}_i^n + \mathbf{S}_i^n \,, \tag{4.10}$$

where

$$\Delta\mathbf{U}_i = \mathbf{U}_i^{n+1} - \mathbf{U}_i^n \,,$$

$$\mathbf{B}_i^n = -\tfrac{1}{\Delta t}\mathbf{P}_i^n \left[\mathbf{U}_i^n - \mathbf{U}_i^m\right] \,,$$

$$\mathbf{C}_i^n = -\tfrac{1}{2\Delta x}A_i^n \left[\mathbf{U}_{i+1}^n - \mathbf{U}_{i-1}^n\right] \,,$$

$$\mathbf{D}_i^n = \tfrac{1}{2\Delta x}\mathbf{P}_i^n \left[\mathbf{U}_{i+1}^n - 2\mathbf{U}_i^n + \mathbf{U}_{i-1}^n\right] \,,$$

$$\mathbf{S}_i^n = \mathbf{P}_i^n \mathbf{S}_i^n \,.$$

A similar method, using implicit-Euler time marching for the pseudo-time iteration would be

$$\Delta\mathbf{U}_i = \mathbf{B}_i^{n+1} + \mathbf{C}_i^{n+1} + \mathbf{D}_i^{n+1} + \mathbf{S}_i^{n+1} \,. \tag{4.11}$$

As was expected, in Equation (4.11), the change in $\mathbf{U}$ from time step n to $n+1$ is calculated based on the values of the other terms evaluated at time $n+1$. Since all the terms on the right-hand side of Equation (4.11) are highly non-linear functions, this represents a large set of coupled non-linear equations that would be very difficult to solve. To avoid this, all

the terms on the right-hand side are instead linearized with respect to their values at time step n (which can be easily computed explicitly) as

$$\mathbf{B}_i^{n+1} = \mathbf{B}_i^n - \tfrac{1}{\Delta t}\mathbf{P}_i^n \Delta \mathbf{U}_i \,, \tag{4.12}$$

$$\mathbf{C}_i^{n+1} = \mathbf{C}_i^n - \tfrac{1}{2\Delta x} A_i^n \left[\Delta \mathbf{U}_{i+1} - \Delta \mathbf{U}_{i-1}\right] \,, \tag{4.13}$$

$$\mathbf{D}_i^{n+1} = \mathbf{D}_i^n + \tfrac{1}{2\Delta x}\mathbf{P}_i^n \left[\Delta \mathbf{U}_{i+1} - 2\Delta \mathbf{U}_i + \Delta \mathbf{U}_{i-1}\right] \,, \tag{4.14}$$

$$\mathbf{S}_i^{n+1} = \mathbf{S}_i^n + \left(\tfrac{\partial \mathbf{S}_i}{\partial \mathbf{U}_i}\right)^n \Delta \mathbf{U}_i \,. \tag{4.15}$$

Assuming $\mathbf{P}$ and A are constant in respect $\mathbf{U}$. The derivative term in the Equation (4.15) can also be found analytically as

$$\frac{\partial \mathbf{S}}{\partial \mathbf{U}} = \begin{bmatrix} 0 & 0 & 0 & 0 & 0 \\ 0 & 0 & 0 & 0 & 0 \\ 0 & 0 & 0 & 0 & 0 \\ \beta_1 & \beta_2 & \beta_3 & \beta_4 & 0 \\ \beta_5 & \beta_6 & \beta_7 & 0 & \beta_8 \end{bmatrix} \,, \tag{4.16}$$

where

$$\beta_1 = -\tfrac{u\left(-\rho u^2+3p\right)}{\rho\tau} \,, \tag{4.17}$$

$$\beta_2 = \tfrac{-3\rho u^2+3p}{\rho\tau} \,, \tag{4.18}$$

$$\beta_3 = \tfrac{3u}{\tau} \,, \tag{4.19}$$

$$\beta_4 = -\tfrac{1}{\tau} \,, \tag{4.20}$$

$$\beta_5 = -\tfrac{3p^2}{\tau\rho^2} + \tfrac{4qu}{\rho\tau} + \tfrac{6pu^2}{\tau\rho} - \tfrac{4u^2\left(-\rho u^2+3p\right)}{\rho\tau} - \tfrac{u\left(-\rho u^3+4q\right)}{\rho\tau} \,, \tag{4.21}$$

$$\beta_6 = -\frac{4q}{\rho\tau} - \frac{12pu}{\tau\rho} + \frac{4u\left(-3\rho u^2+3p\right)}{\rho\tau} + \frac{4\rho u^3+4q}{\rho\tau}\,, \tag{4.22}$$

$$\beta_7 = \frac{6p}{\rho\tau} + \frac{6u^2}{\tau}\,, \tag{4.23}$$

$$\beta_8 = -\frac{1}{\tau}\,. \tag{4.24}$$

These can be used to rewrite Equation (4.11) as

$$\begin{aligned}\Delta\mathbf{U}_i = &-\frac{\Delta\tau}{\Delta t}\mathbf{P}_i^n\Delta\mathbf{U}_i - \frac{\Delta\tau}{\Delta t}\mathbf{P}_i^n\left(\mathbf{U}_i^n - \mathbf{U}_i^m\right) - \frac{\Delta\tau}{2\Delta x}\mathbf{A}_i^n\left(\Delta\mathbf{U}_{i+1} - \Delta\mathbf{U}_{i-1}\right)\\ &-\frac{\Delta\tau}{2\Delta x}\mathbf{A}_i^n\left(\mathbf{U}_{i+1} - \mathbf{U}_{i-1}\right) + \frac{\Delta\tau}{2\Delta x}\mathbf{P}_i^n\left(\Delta\mathbf{U}_{i+1} - 2\Delta\mathbf{U}_i + \Delta\mathbf{U}_{i-1}\right)\\ &+\frac{\Delta\tau}{2\Delta x}\mathbf{P}_i^n\left(\mathbf{U}_{i+1} - 2\mathbf{U}_i + \mathbf{U}_{i-1}\right) + \Delta\tau\mathbf{P}_i^n\frac{\partial\mathbf{S}_i}{\partial\mathbf{U}_i}\Delta\mathbf{U}_i + \Delta\tau\mathbf{P}_i^n\mathbf{S}_i^n\,.\end{aligned} \tag{4.25}$$

Clearly, the time update for one point is coupled to the update for all other points. However, this equation is now linearized and can be more easily handled. The discrete Equation (4.25) can be written in standard form as

$$\mathbf{J}\mathbf{x} = \mathbf{b}\,. \tag{4.26}$$

Here, the matrix, $\mathbf{J}$ has the form

$$\mathbf{J} = \begin{bmatrix} [\mathbf{X}_0] & [\mathbf{Z}_0] & 0 & 0 & 0 & \dots & 0 \\ [\mathbf{Y}_1] & [\mathbf{X}_1] & [\mathbf{Z}_1] & 0 & 0 & \dots & 0 \\ \dots & \dots & \dots & \dots & \dots & \dots & \dots \\ 0 & 0 & 0 & \dots & 0 & [\mathbf{Y}_m] & [\mathbf{X}_m] \end{bmatrix}. \tag{4.27}$$

$\mathbf{J}$ is therefore a block tri-diagonal matrix with

$$\mathbf{X}_i = \tfrac{1}{\Delta\tau}\mathbf{I} + \tfrac{1}{\Delta x}\mathbf{P}_i + \tfrac{1}{\Delta t}\mathbf{P}_i - \mathbf{P}_i\tfrac{\partial \mathbf{S}_i}{\partial \mathbf{U}_i}\,,$$

$$\mathbf{Y}_i = -\tfrac{1}{2\Delta x}\mathbf{P}_i - \tfrac{1}{2\Delta x}\mathbf{A}_i\,,$$

$$\mathbf{Z}_i = -\tfrac{1}{2\Delta x}\mathbf{P}_i + \tfrac{1}{2\Delta x}\mathbf{A}_i\,.$$

$\mathbf{I}$ is the 5×5 identity matrix. Similarly, $\mathbf{b}$ and $\mathbf{x}$ are vectors given by

$$\mathbf{b} = \begin{pmatrix} \mathbf{B}_0 + \mathbf{C}_0 + \mathbf{D}_0 + \mathbf{S}_0 \\ \mathbf{B}_1 + \mathbf{C}_1 + \mathbf{D}_1 + \mathbf{S}_1 \\ \vdots \\ \mathbf{B}_i + \mathbf{C}_i + \mathbf{D}_i + \mathbf{S}_i \\ \vdots \\ \mathbf{B}_m + \mathbf{C}_m + \mathbf{D}_m + \mathbf{S}_m \end{pmatrix}, \qquad \mathbf{x} = \begin{pmatrix} \Delta\mathbf{U}_0 \\ \Delta\mathbf{U}_1 \\ \vdots \\ \Delta\mathbf{U}_i \\ \vdots \\ \Delta\mathbf{U}_m \end{pmatrix}. \tag{4.28}$$

Here, m denotes the number of cells in the mesh. Since $\mathbf{J}$ is a block tri-diagonal matrix, one can easily solve it directly with simple specialized algorithms for banded matrices. For time-accurate problems, Δt is chosen based on the physical behaviour of the problem and held constant in the current study. For steady-state problems, Δt starts at a prescribed value and, as the solution gets close to the steady state, it is possible to increase the value of Δt. As for $\Delta\tau$, it is calculated based on the maximum wavespeed of the system as follows

$$\Delta\tau = \mathrm{CFL}\left(\frac{\Delta x}{\lambda_{max}}\right), \tag{4.29}$$

where CFL is the classical time-step restriction for explicit methods [25]. In the current

work, the CFL number is calculated for each pseudo time iteration by

$$\text{CFL} = \frac{10^5}{|\Delta \mathbf{U}|}, \tag{4.30}$$

where $|\Delta \mathbf{U}|$ is the 1-norm of the update vector. As can be seen, the smaller $\Delta \mathbf{U}$ becomes, the bigger the CFL number gets, which helps to get to the steady-state solution faster.

4.3.2 Construction of Dimensional Matrix A

In order to solve Equation (4.25), the matrix, $\mathbf{A}$, must be built. The in-depth study of the preconditioner and flux Jacobian in Chapter 3 was in a non-dimensionalized setting with zero bulk velocity. The general matrix, $\mathbf{A}$, can be expressed in terms of the entries in the non-dimensional flux Jacobian as

$$\mathbf{A} = \begin{bmatrix} 0 & 1 & 0 & 0 & 0 \\ 0 & 0 & 1 & 0 & 0 \\ 0 & 0 & 0 & 1 & 0 \\ 0 & 0 & 0 & 0 & 1 \\ \psi_0 & \psi_1 & \psi_2 & \psi_3 & \psi_4 \end{bmatrix}, \tag{4.31}$$

with

$$\psi_0 = \left[a_0 \left(\frac{p}{\rho}\right)^{\left(\frac{5}{2}\right)} - a_1 \left(\frac{p}{\rho}\right)^2 u + a_2 \left(\frac{p}{\rho}\right)^{\left(\frac{3}{2}\right)} u^2 - a_3 \left(\frac{p}{\rho}\right) u^3 + a_4 \left(\frac{p}{\rho}\right)^{\left(\frac{1}{2}\right)} u^4 + u^5 \right] W^5,$$

$$\psi_1 = \left[a_1 \left(\frac{p}{\rho}\right)^2 - 2a_2 \left(\frac{p}{\rho}\right)^{\left(\frac{3}{2}\right)} u + 3a_3 \left(\frac{p}{\rho}\right) u^2 - 4a_4 \left(\frac{p}{\rho}\right)^{\left(\frac{1}{2}\right)} u^3 - 5u^4 \right] W^4,$$

$$\psi_2 = \left[a_2 \left(\frac{p}{\rho}\right)^{\left(\frac{3}{2}\right)} - 3a_3 \left(\frac{p}{\rho}\right) u + 6a_4 \left(\frac{p}{\rho}\right)^{\left(\frac{1}{2}\right)} u^2 + 10u^3 \right] W^3,$$

$$\psi_3 = \left[a_3 \left(\frac{p}{\rho} \right) - 4a_4 \left(\frac{p}{\rho} \right)^{\left(\frac{1}{2}\right)} u - 10u^2 \right] W^2 \,,$$
$$\psi_4 = \left[a_4 \left(\frac{p}{\rho} \right)^{\left(\frac{1}{2}\right)} + 5u \right] W \,,$$

where the a's are the entries given in Equations (3.6) to (3.10) and W is given by Equation (3.42).

Chapter 5

Numerical Results

This chapter discusses the numerical results that are used to verify and validate the proposed preconditioned 5-moment closure and its numerical solution. Section 1 verifies that the behaviour of the wavespeeds of the proposed system are indeed altered and remain finite as compared to the non-preconditioned 5-moment system for moment states encountered during the computation of a typical Riemann problem. Section 2 discusses the validation of the steady-state solution of the model for the prediction of stationary shock-waves profile. Comparisons to known results derived by the original 5-moment system, Euler equations, Navier-Stokes equations and direct numerical solution of the Boltzmann equation using BGK collision operator results are made. In Section 3, results of time-accurate calculations for Riemann problems with different levels of non-equilibrium are compared for the preconditioned 5-moment system, the Euler equations, the Navier-Stokes equations and direct solution of the BGK equation.

5.1 Numerical Verification

The main goal of the preconditioning is the elimination of arbitrarily large fluxes and wavespeeds near the Junk singular line. To verify that this has been accomplished and to see its effect on practical situations, two Riemann problems are considered. Both comprise the up- and down-stream states of stationary shock waves, one with an upstream Mach number of 2 and the one with a Mach number of 4. The dual time stepping strategy explained in the previous chapter is used to advance the calculation to a time of $t = 0.007$ s. Wavespeeds are then determined by numerically computing the eigenvalues of the flux Jacobian of the original and preconditioned systems. As is expected, for both Riemann problems, wavespeeds related to the non-preconditioned 5-moment system become extremely large, four orders of magnitude larger than those of the initial conditions. As a result, explicit time marching would become impossible in this scheme since the local time step is determined by the maximum wavespeed of the system. However, the preconditioned system offers wavespeeds that remain of the same order of magnitude as the initial ones. The system does not become increasingly stiff as time advances. Figure 5.1 shows the wavespeeds of both the preconditioned and the original 5-moment closure for these two problems. The wavespeeds of the preconditioned system are clearly better controlled.

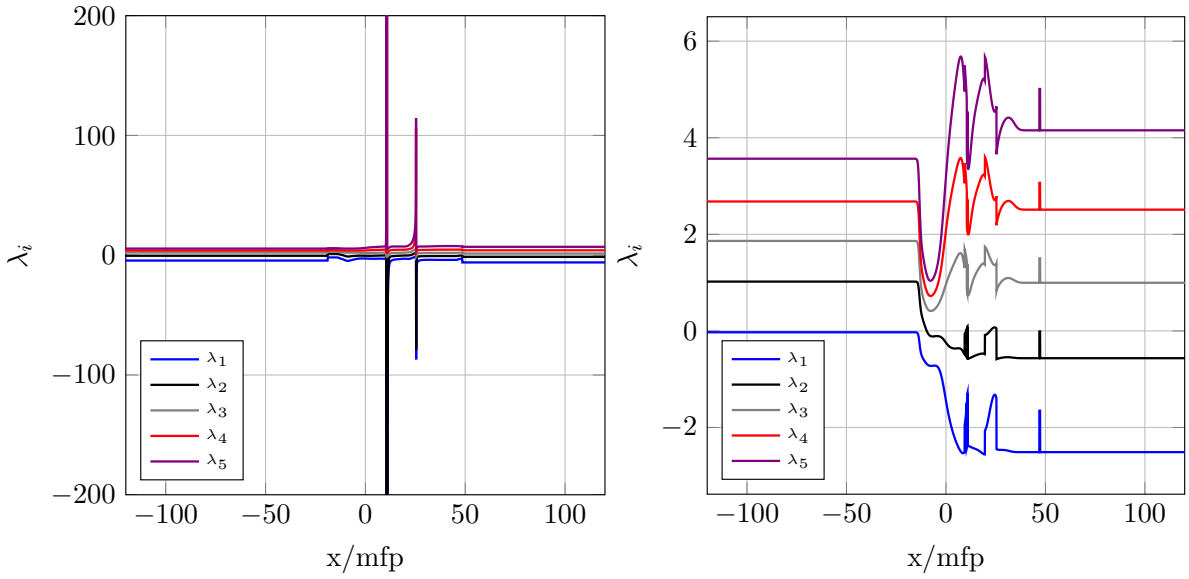

(a) $Ma = 2$ (b) $Ma = 2$

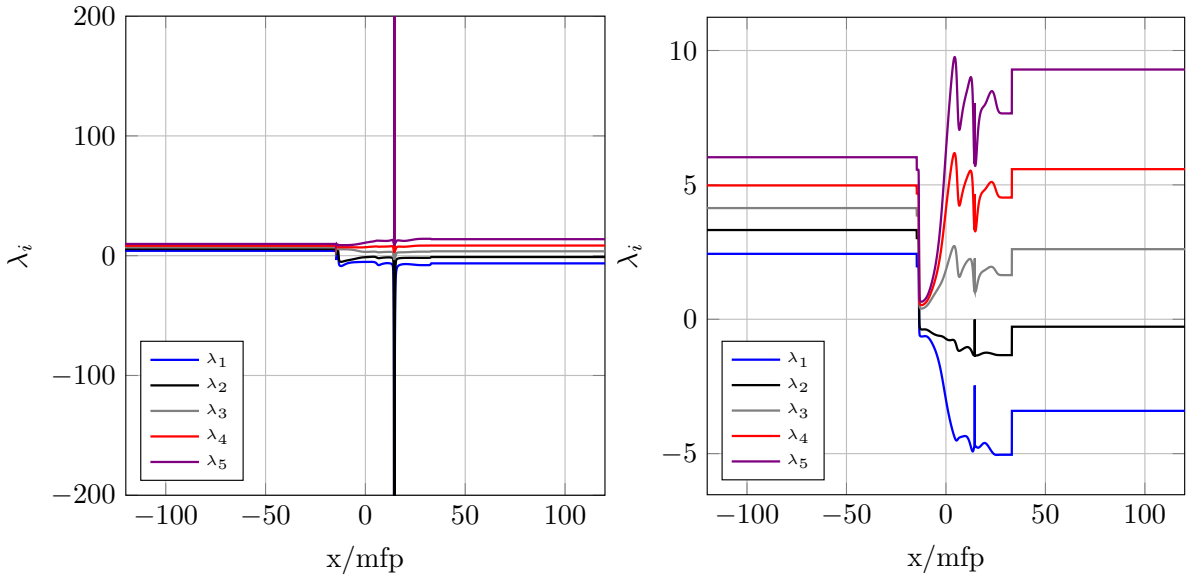

(c) $Ma = 4$ (d) $Ma = 4$

Figure 5.1: *Comparison of wavespeeds of the original 5-moment closure to the preconditioned one for a typical Riemann problem.*

It is interesting to plot the solutions of these problems in $q_\star$-$r_\star$ space to see how close the solution comes to the Junk line. This is shown in Figure 5.2. It can be clearly seen in Figure 5.2a, for the problem with Ma = 2, while the numerical computation is evolving to a steady-state solution, the system crosses the Junk line, which as expected and shown in Figure 5.1a results to infinitely large wavespeeds of the non-preconditioned system. As a result, time marching would no longer be possible. Also, for a shock problem with Ma = 4, the unsteady solution at this time of the 5-moment system does not cross the Junk line, however, it does come very close. Again, in this situation, solution of the non-preconditioned system would become impossible.

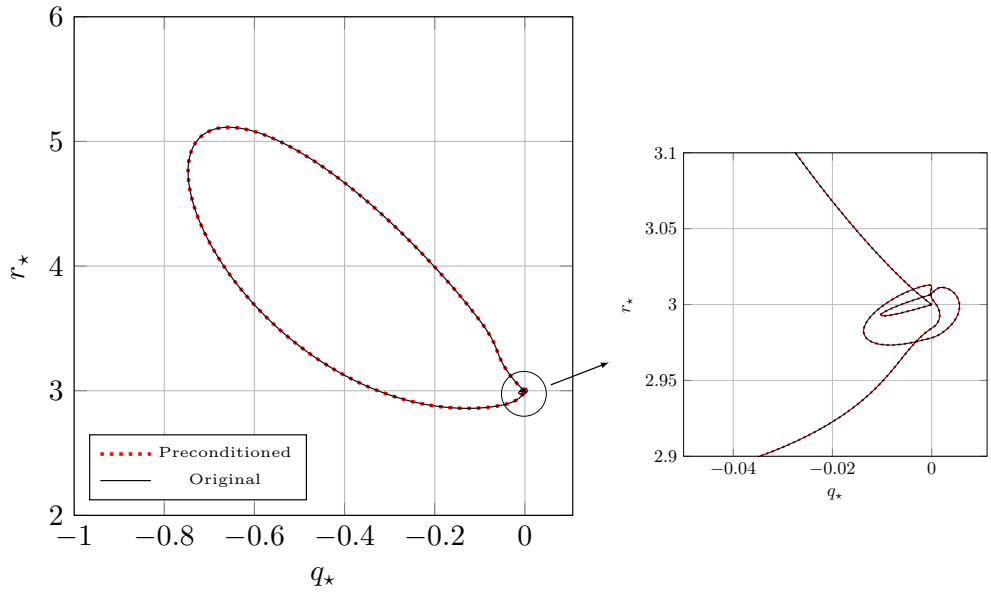

(a) $Ma = 2$

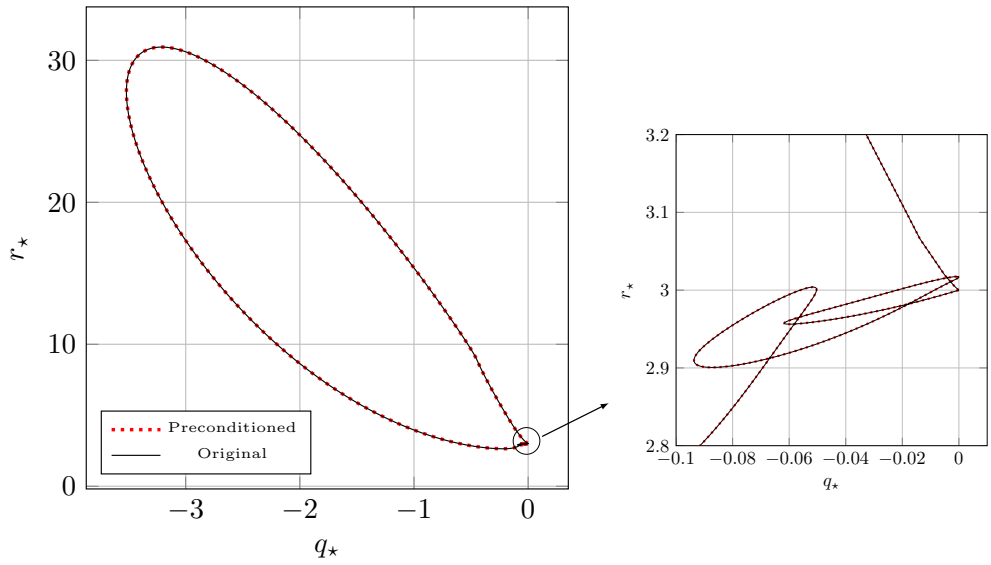

(b) $Ma = 4$

Figure 5.2: *States of the original and preconditioned systems in the physically realizable region for a time-accurate solution.*

5.2 Numerical Validation for Practical Problems

After verifying that the preconditioned system efficiently controls the arbitrarily large wavespeeds of the original system, one needs to show that the preconditioned system does in fact yield the same steady-state solution as the non-preconditioned 5-moment system. In order to do that, a numerical investigation of the internal structure of stationary shock waves is carried out. Solutions obtained with the preconditioned 5-moment system are studied and compared with results obtained using the non-preconditioned system. These results from the non-preconditioned equations were previously obtained with a code that contains many hard-coded limits and switches to try to control the singularity in the system. These limits must often be tuned for the particular problem, and convergence is severely limited by the extremely high wavespeeds in the system. Comparisons are also made to the direct numerical solution of the BGK equation (the full kinetic equation with the BGK collision operator) and the Navier-Stokes-like equations that result from a Chapman-Enskog expansion for this one-dimensional gas [21],

$$\frac{\partial \rho}{\partial t} + \frac{\partial}{\partial x}\left(\rho u\right) = 0\,, \tag{5.1}$$

$$\frac{\partial}{\partial t}\left(\rho u\right) + \frac{\partial}{\partial x}\left(\rho u^2 + p\right) = 0\,, \tag{5.2}$$

$$\frac{\partial}{\partial t}\left(\rho u^2 + p\right) + \frac{\partial}{\partial x}\left(\rho u^3 + 3up\right) - \frac{\partial}{\partial x}\left(3p\tau\frac{\partial}{\partial x}\left(\frac{p}{\rho}\right)\right) = 0\,. \tag{5.3}$$

These equations can be regarded as the continuum (Navier-Stokes) model for one-dimensional physics. Pre-existing computational codes for the direct solution of the BGK equation and the Navier-Stokes-like equations were used.

In the current work, for the stationary shock problems, the upstream values of pressure

and density are taken to be standard atmospheric values, 101325 Pa and 1.225 kg/m^3, respectively. The problems begins with a discontinuity in the middle of the domain, where the Rankine-Hugoniot jump conditions are used to calculate the downstream flow conditions for shock waves of varying Mach numbers. As mentioned before, the BGK collision operator is used and the relaxation time is held fixed at a value of $\tau = 10^{-7}s$ for all computations. This is not physically accurate but allows the behaviour of the left-hand side to be studied with the simplest possible collision operator. Based on these values, the mean free path, λ, is taken to be

$$\lambda = \frac{16\tau}{5}\sqrt{\frac{p}{2\pi\rho}} = 3.67 \times 10^{-5}\,\mathrm{m}\,. \tag{5.4}$$

Equation (5.4) is derived from the expression for hard-sphere collisional processes given by Bird [2],

$$\lambda = \frac{16\mu}{5\sqrt{2\pi\rho p}}\,, \tag{5.5}$$

where the relaxation time and fluid viscosity for the BGK collision operator are related by

$$\mu = \tau p\,. \tag{5.6}$$

Equation (5.6) is not completely accurate for the one-dimensional gas as it was derived for three-dimensional physics. However, in the current study, the mean free path is only used to non-dimensionalized the x axis in the following results and this estimate for the mean free path is considered to give an accurate estimate of the length scales involved in each problem. The solutions are insured to be grid-converged. The domain of the problems is made up of 5000 cells with equal spacing, which is more than enough to have grid independence. The boundary conditions are held constant and equal to the initial condition. Table 5.1

gives detailed information for the problems set up. As for the convergence rate, in both the physical and pseudo time step loop, $|\Delta \mathbf{U}|$ between two successive time steps must be less than 10^{-8} for the solution to be deemed converged.

Table 5.1: Shock structure problem for Mach 2, 4, and 8.

Boundary Condition	Fixed
Domain size	-0.005 m $\leq x \leq 0.005$ m
Mesh Resolution	5000 cells
Upstream Flow Density (ρ_1)	1.225 kg/m^3
Upstream Flow Pressure (p_1)	101325 Pa
Heat Capacity Ratio (γ)	3

Figure 5.3 shows the numerical solutions of the preconditioned 5-moment closure as compared to the solutions to the non-preconditioned 5-moment closure, the one-dimensional Navier-Stokes-like equation and the direct numerical solution of the BGK equation for stationary shock waves with upstream Mach numbers of 2, 4, and 8. Plots of normalized density such that it transitions from 0 to 1, and non-dimensional heat flux, $q_\star$, are shown. It can be clearly seen that the preconditioning strategy is validated as the results derived from the preconditioned and non-preconditioned 5-moment system are exactly the same. Also, the solutions of the 5-moment closure are in far better agreement with the direct solution of the kinetic equation compared to the ones derived from Navier-Stokes for all Mach numbers. As can be observed, the non-equilibrium effects become stronger and stronger as the Mach number increases. The Navier-Stokes solutions quickly become worse and worse, whereas the moment solutions still remain very close to the BGK equation solutions across the full range of Mach number considered. The superiority of the moment-closure-based technique is very clearly seen for this non-equilibrium case.

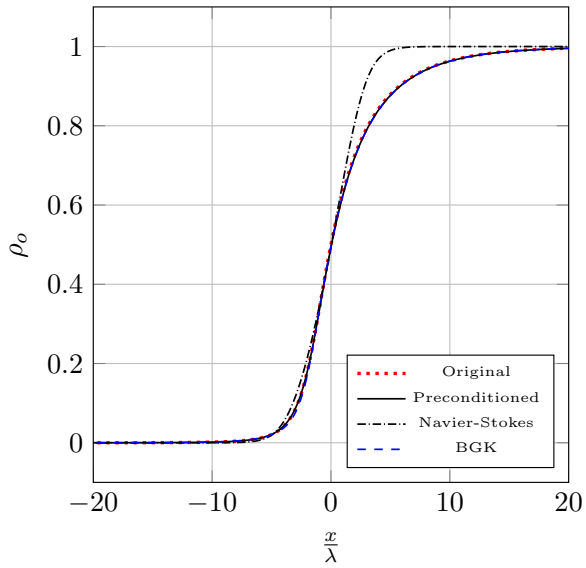

(a) *Normalized density,* $Ma = 2$

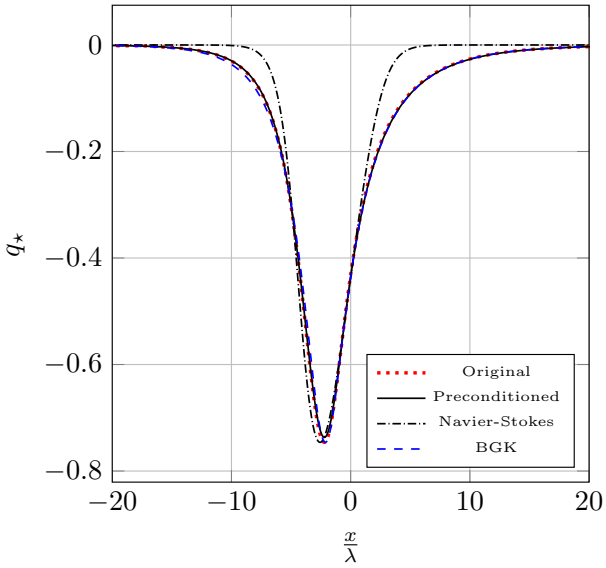

(b) *Non-dimensionlized heat flux,* $Ma = 2$

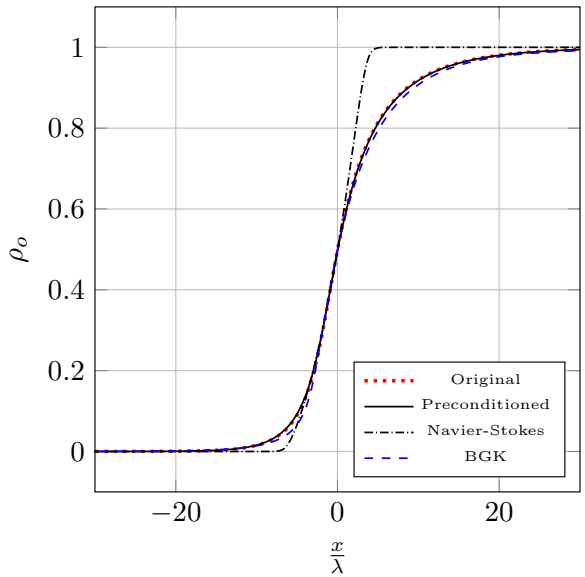

(c) *Normalized density,* $Ma = 4$

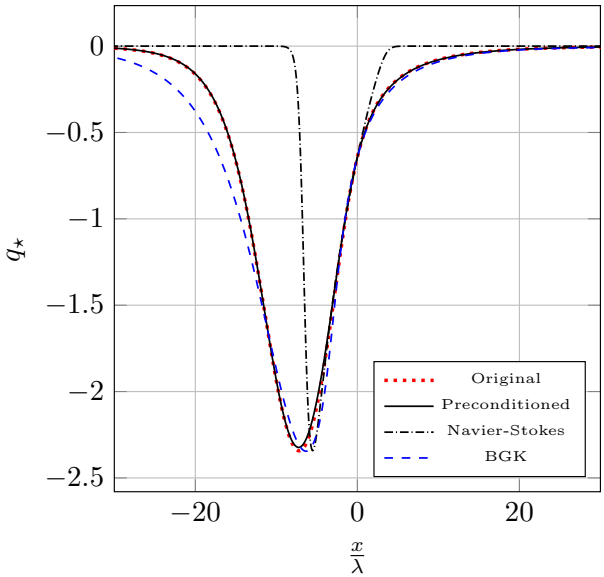

(d) *Non-dimensionlized heat flux,* $Ma = 4$

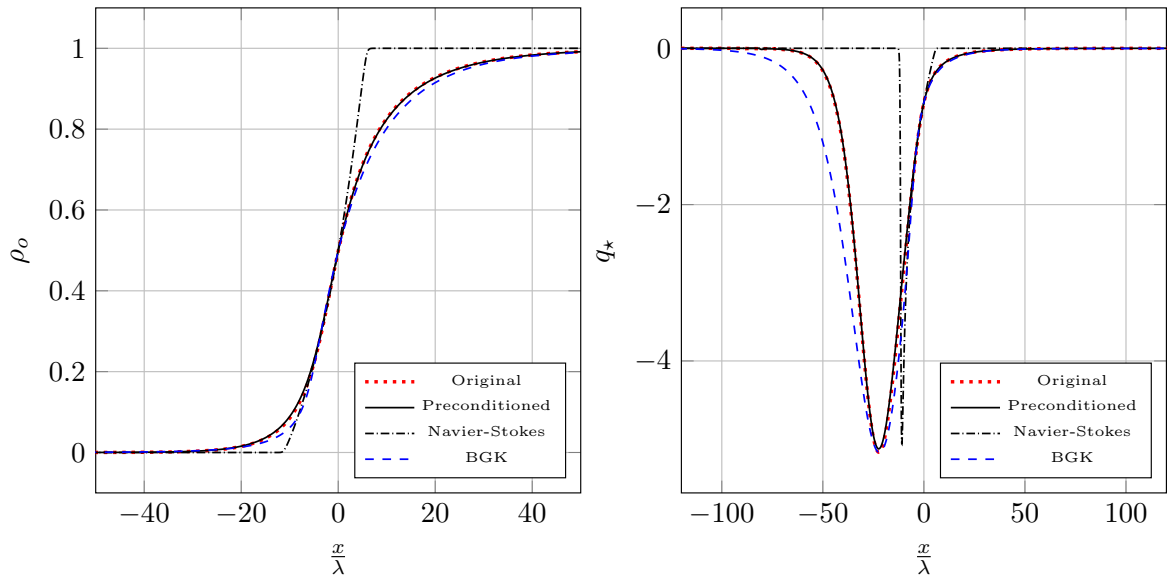

(e) *Normalized density, Ma = 8*

(f) *Non-dimensionlized heat flux, Ma = 8*

Figure 5.3: *Predicted normalized density and non-dimensionalized heat-transfer through a stationary shock wave for a one-dimensional gas as determined using the original non-preconditioned 5-moment closure, preconditioned 5-moment closure, Navier-Stokes-like equations, and direct numerical solution of the BGK kinetic equation.*

5.3 Numerical Results for a Riemann Problem

In order to study the behaviour of the preconditioned 5-moment closure, more Riemann initial-value problems are considered across a range of Knudsen numbers. Such problems could not be reliably computed with the non-preconditioned system of equations. Each problem of interest consists of the same two-state initial condition with a density ratio of almost 0.3, pressure ratio of 0.25, and an initial velocity of zero. The two states are initially separated from each other using a diaphragm in the middle of the domain of the interest. It is assumed at $t = 0$, the diaphragm is suddenly raptured and causes a discontinuity between the two states. Here also, the boundary conditions are held constant and equal to the initial values. The domain is 0 m $\leq x \leq$ 1 m and this length of 1 m is taken as the characteristic length to estimate the Knudsen number of each problem. The mean

Table 5.2: Riemann problem condtion for different relaxation time.

Boundary Condition	Fixed
Domain size	$0 \text{ m} \leq x \leq 1 \text{ m}$
Mesh Resolution	3000 cells
Left State Density (ρ_l)	4.696 kg/m^3
Left State Velocity (u_l)	0 m/s
Left State Pressure (p_l)	404400 Pa
Right State Density (ρ_r)	1.408 kg/m^3
Right State Velocity (u_r)	0 m/s
Right State Pressure (p_r)	101100 Pa

free path is again calculated using Equation (5.4). Six different situations were studied corresponding to Knudsen numbers of 1.1×10^{-4}, 1.1×10^{-3}, 1.1×10^{-2}, 1.1×10^{-1}, 1.1, and 1.1×10^{1}, therefore, all three regimes (continuum , transition and free molecular) are investigated. The Knudsen number is adjusted by changing the relaxation time, τ. In each case, a grid with 3000 equally spaced cells is used. Table 5.2 gives more information for these problems. The resulting solutions are presented in Figure 5.4. A comparison is made between the preconditioned 5-moment closure, the Euler equations, high-resolution direct numerical solution of the BGK equation, and numerical solution of the equivalent Navier-Stokes-like equation, as shown in the previous section.

It can be seen in Figures 5.4a, 5.4b, 5.4c, and 5.4d that, in the continuum regime, all three non-equilibrium solution treatments give solutions that are virtually identical to the solution of the Euler equations. This is expected since, in this regime, non-equilibrium effects on the gas are negligible. It can also be seen in Figures 5.4b, and 5.4d that, in the continuum limit, the 5-moment system and Navier-Stokes-like equations predict a heat-flux that is in good agreement with the reference BGK solution. All three of these models give physically accurate predictions in this regime.

Figures 5.4e, 5.4f, 5.4g, 5.4h, 5.4i, and 5.4j show the numerical results for the transition regime. As can be seen, the Euler equations give the same answer for all three different Knudsen numbers as they have absolutely no treatment of non-equilibrium effects. In Figures 5.4e, and 5.4f, the solutions of the 5-moment system and the Navier-Stokes-like equations still remain close to the ones derived by the BGK equation. However, it is clear that, as the Knudsen number increases, increasing non-equilibrium effects become present and both methods become less and less accurate, as compared to the BGK solution. Despite this, it can be observed that, the 5-moment closure still gives a solution that is in a better agreement to the BGK solution for both normalized density and non-dimensionlized heat flux in this regime than the Navier-Stokes model.

Finally, Figures 5.4k and 5.4l present results for the nearly free-molecular regime. As was expected, the Euler equation again yields the same answer as those for the continuum regime. Since in this regime, collisions between particles become almost negligible, the terms associated with the collision operator become insignificant in the 5-moment system. Therefore, the system behaves completely hyperbolically and, as a result, five distinct wavespeeds appear in the result of the 5-moment system. None of the models agree with the expensive BGK calculation at such high Knudsen numbers. In fact, they all approximate the true continuous transition by discrete waves. The Euler solution again posses the traditional three waves from the continuum regime. As the Navier-Stokes equations massively over-predict heat transfer in this regime, the solution they predict actually approaches the two-wave solution of the isothermal Euler equations. At such high Knudsen numbers, it actually gives worse predictions than the Euler equations for this case. The

five-wave solution of the moment model remains significantly closer to the reference solution than either continuum model and does provide some level of physically realistic approximation, even at these extreme Knudsen numbers.

A comparison is also made between the 5-moment system and traditional models with regards to their computational cost. It is observed that for high-Knudsen numbers flows, the 5-moment system is cheaper, whereas for gas flows with low Knudsen numbers, the traditional models tend to be less expensive. However, it should be kept in mind that the numerical scheme used in this research for solving the preconditioned 5-moment system is not optimized. A detailed comparison of the cost related to each model would require further study.

It is interesting to plot the solutions of some of these problems in $q_\star$-$r_\star$ space to see how far these problems depart from the local equilibrium during their evolution. It is also interesting to see if the gas state crosses the Junk line for this situation. Results from the 5-moment system are only compared with the BGK equation since the Navier-Stokes equation do not give any prediction for fourth moment, $r_\star$. It can be observed that the level of agreement between the two models reduces as the Knudsen number rises. It is also interesting to note that deviations seem to increase when the BGK reference solution crosses the Junk line, which happens at higher Knudsen numbers. In regions where the BGK solution is far from the Junk line, agreement is better.

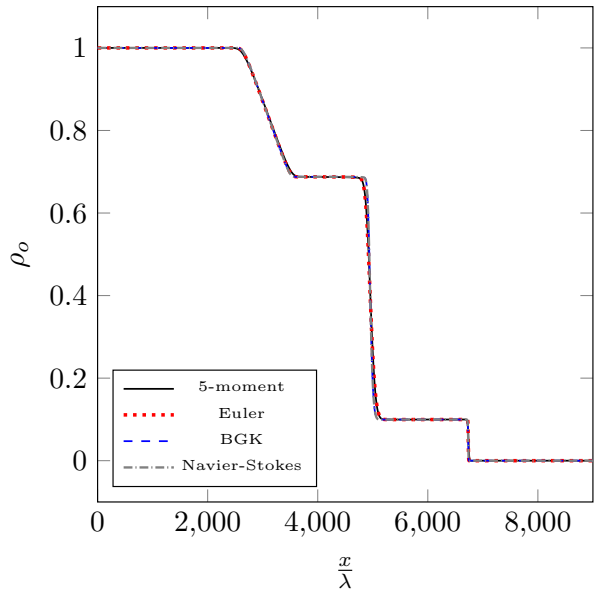

(a) $Kn = 1.1 \times 10^{-4}$

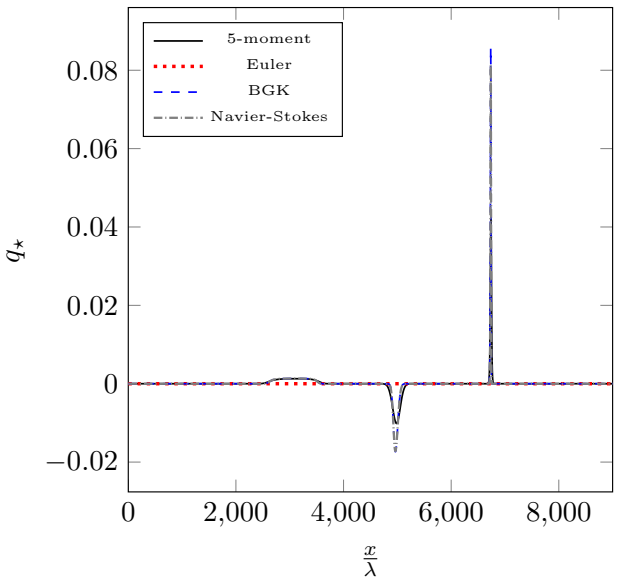

(b) $Kn = 1.1 \times 10^{-4}$

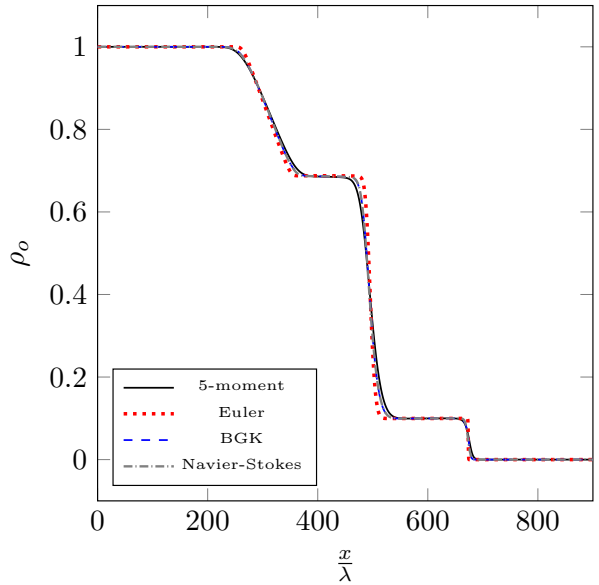

(c) $Kn = 1.1 \times 10^{-3}$

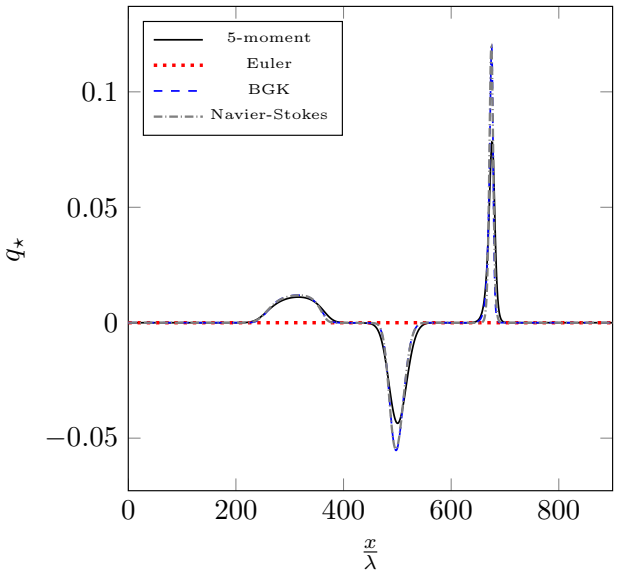

(d) $Kn = 1.1 \times 10^{-3}$

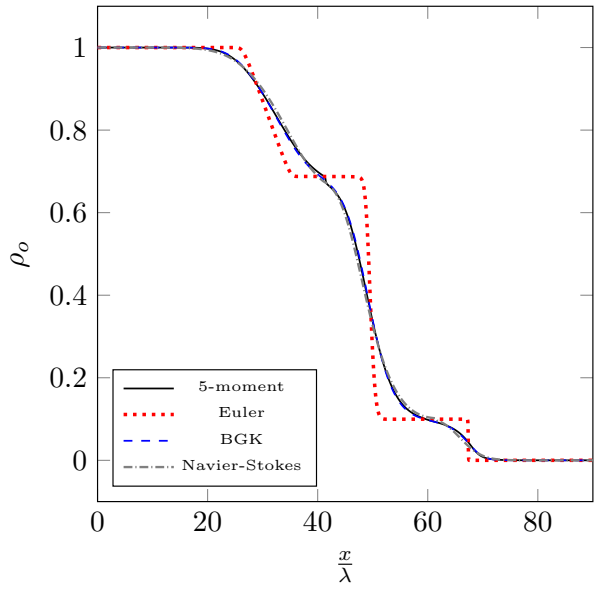

(e) $Kn = 1.1 \times 10^{-2}$

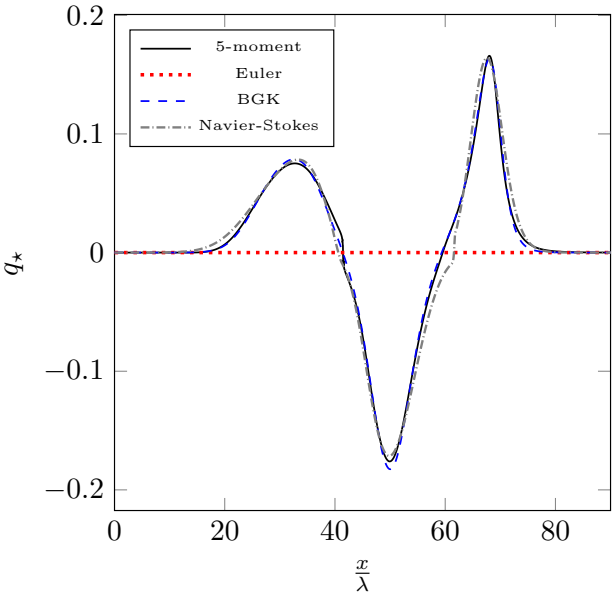

(f) $Kn = 1.1 \times 10^{-2}$

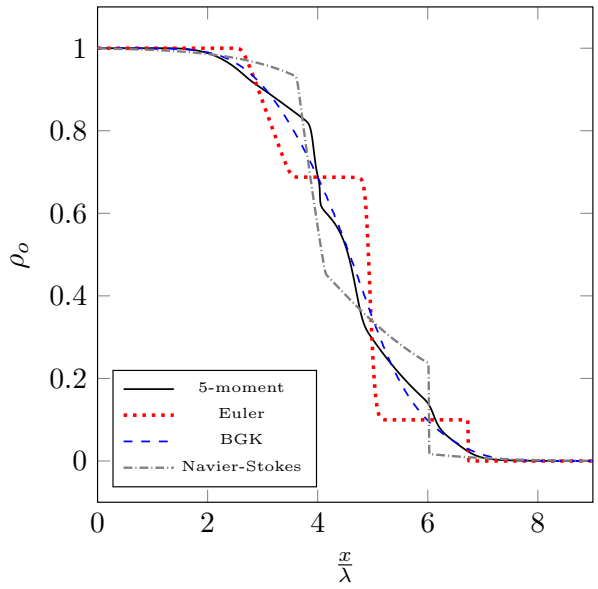

(g) $Kn = 1.1 \times 10^{-1}$

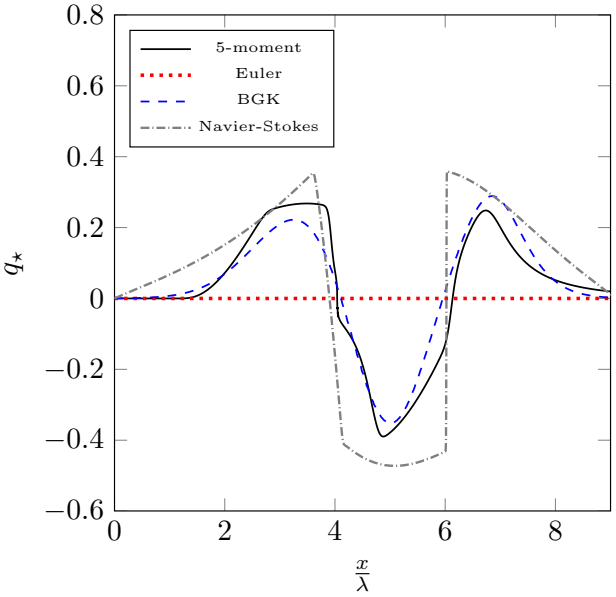

(h) $Kn = 1.1 \times 10^{-1}$

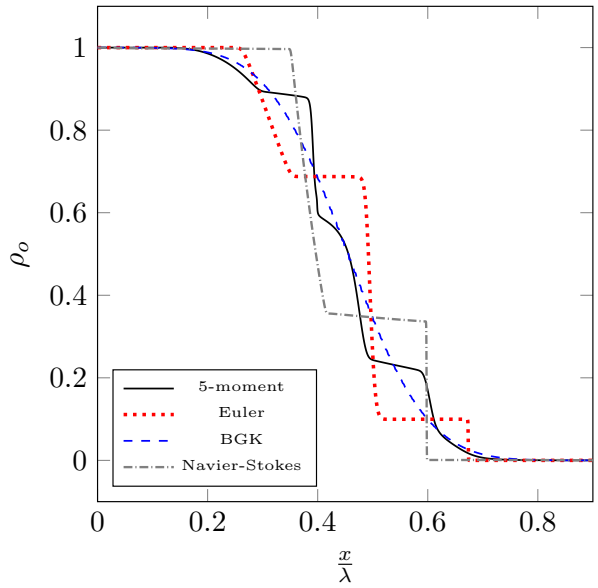

(i) $Kn = 1.1$

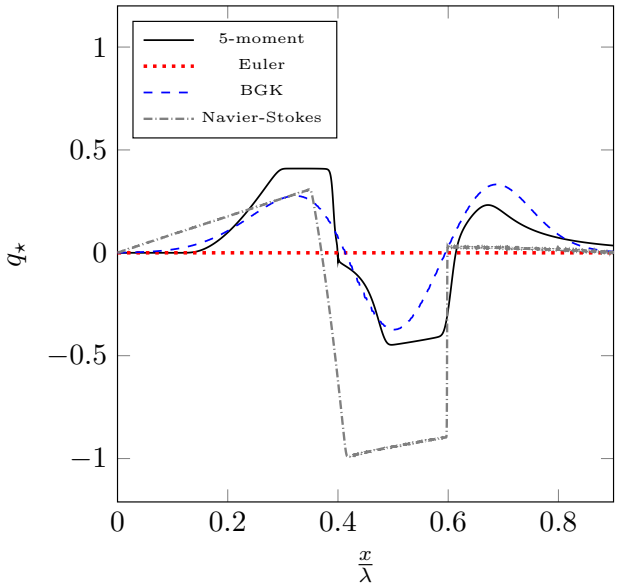

(j) $Kn = 1.1$

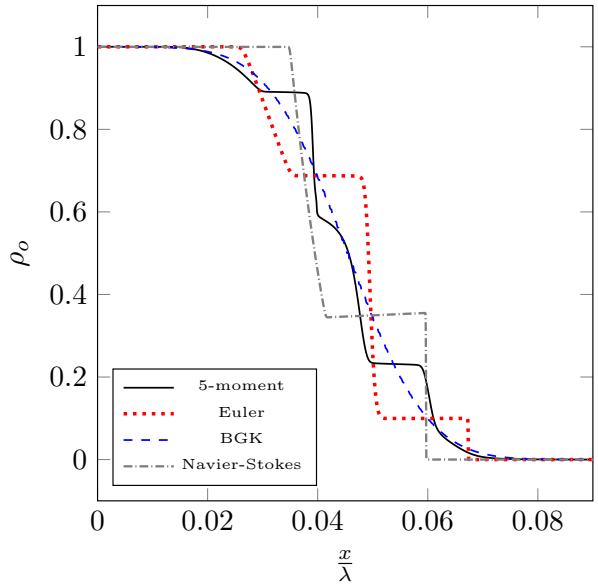

(k) $Kn = 1.1 \times 10^1$

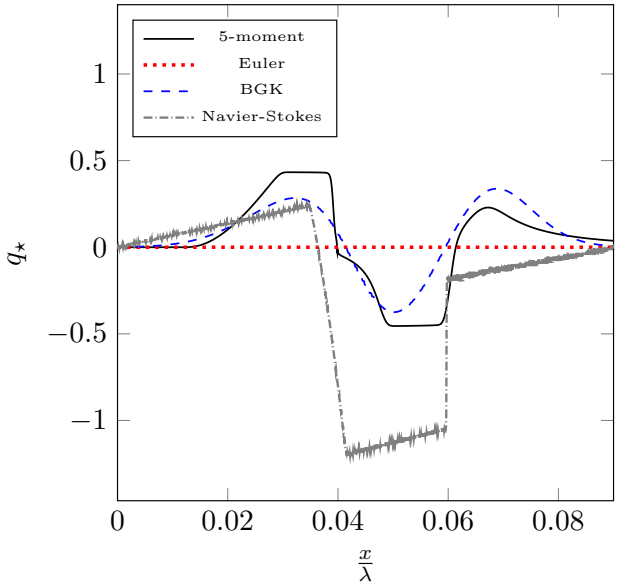

(l) $Kn = 1.1 \times 10^1$

Figure 5.4: *Predicted normalized density and non-dimensionalized heat-transfer for the Riemann initial-value problem for a one-dimensional gas as determined using the preconditioned 5-moment closure, the Euler equations, direct numerical solution of the BGK kinetic equation, and Navier-Stokes-like equations for a range of Knudsen numbers.*

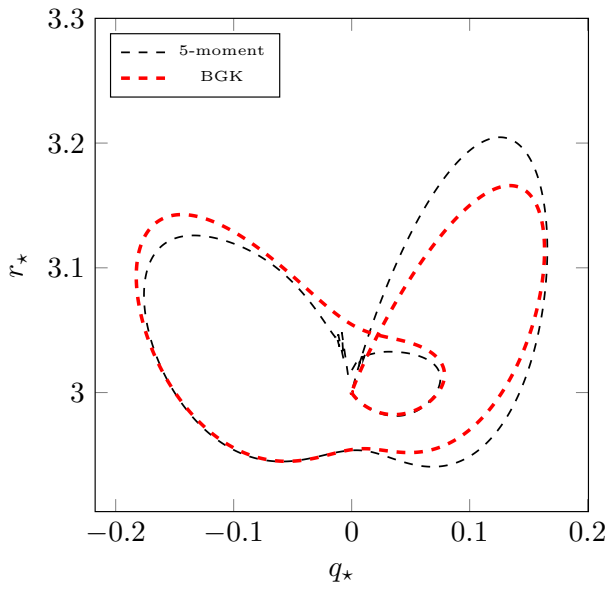

(a) $Kn = 1.1 \times 10^{-2}$

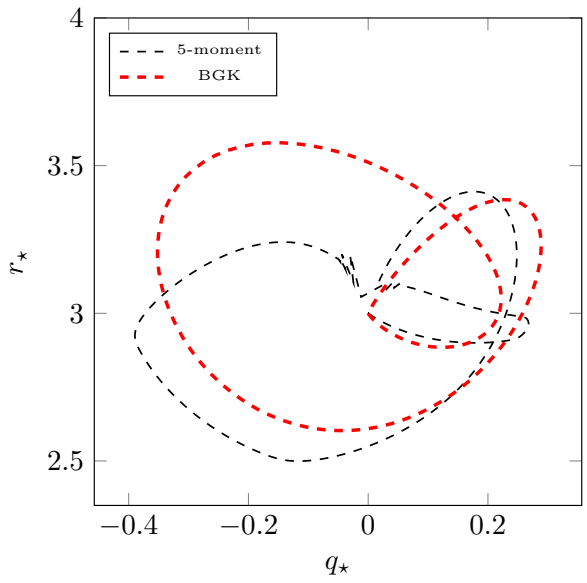

(b) $Kn = 1.1 \times 10^{-1}$

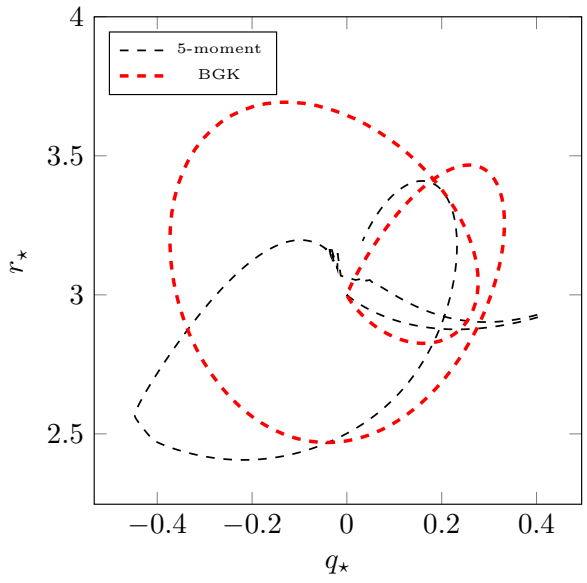

(c) $Kn = 1.1$

Figure 5.5: *Predicted non-dimensionalized heat-transfer and fourth moment for the Riemann initial-value problem for a one-dimensional gas as determined using the preconditioned 5-moment closure and direct numerical solution of the BGK kinetic equation for a range of Knudsen numbers.*

Chapter 6

Conclusions

This study has been concerned with the preconditioning of a new hyperbolic 5-moment closure in order to remove the arbitrarily large values of the closing flux of the system and the wavespeeds without altering the solution of the system during the numerical computation. The resulting system gives a set of hyperbolic non-conservative partial differential equations that can be handled numerically much more easily than the original non-preconditioned system. The new technique offers a robust and efficient method to predict gas behaviour both in and out of local thermodynamic equilibrium. It has been demonstrated that the original non-preconditioned and preconditioned 5-moment closure systems share the same solution for different Riemann initial-value problems. Original contributions are:

- the construction of accurate approximate expressions for the wavespeeds of the original system over the full range of physically possible states,
- the development of a preconditioner for the original 5-moment closure that removes the singularity in the closing flux as the Junk line is approached,

- the numerical implementation of the proposed preconditioned 5-moment system using a stable centred-difference scheme,

- the verification of the preconditioner performance on a practical application by comparing wavespeeds derived from original and preconditioned 5-moment system for an unsteady solution of a Riemann problem,

- the validation of the preconditioned 5-moment steady-state solution with the original 5-moment system, the Navier-Stokes equations, and BGK equation, for predictions of the internal structure of shock waves with different up-stream Mach numbers,

- the comparison of the time-accurate solution of Riemann initial-value problems obtained by the preconditioned 5-moment closure, the Euler equations, the Navier-Stokes equations, and the BGK equation.

The benefits of using the proposed preconditioning strategy on the 5-moment system can be divided into two types: mathematical advantage and numerical advantage. The main mathematical advantage of using the preconditioner is that the closing flux is no longer singular, and the system is defined for all realizable states. The removal of the arbitrarily large wavespeeds leads to numerical solutions that are more efficient and robust.

In Chapter 3, the derivation of an approximation for the eigenvalues of the original 5-moment system is shown. It is based on interpolation between regions where the characteristic polynomial given by the flux Jacobian of the system can be solved explicitly. Furthermore in this Chapter, a preconditioner was developed based on these approximate wavespeeds in order to remove the infinitely large wavespeeds and singular flux from the

system.

Chapter 4 shows the implementation of the preconditioner for the 5-moment system within a numerical scheme for its solution. A centred-difference scheme is proposed based on the Lax-Friedrichs model for discretizing the system. In addition, a dual-time-stepping technique is also introduced and coupled with the finite difference scheme to allow time-accurate behaviour to be modeled and to guarantee the well-posedness of the preconditioned system by keeping its behaviour close to the original one, as much as possible. Finally, the implicit Euler time-marching method is used in the numerical computation to speed up the convergence rate of the scheme.

Chapter 5 presents the numerical results derived from the preconditioned 5-moment system. These solutions are used to verify the effectiveness of the preconditioned system for removing the arbitrarily large wavespeeds from the system and also to validate that the steady-state solution of the system is not altered by the preconditioner. The accuracy of the 5-moment system in different flow regimes is investigated by comparing to the Euler equations, the Navier-Stokes equations, and BGK equation for a typical Riemann problem.

6.1 Suggestion and Future Work

This study has clearly demonstrated that the idea of using a preconditioner to scale the wavespeeds of the original 5-moment system is effective. However, the proposed preconditioner results in a system that cannot be written in a conservation form, which is found to be much harder to deal with numerically compared to conservative hyperbolic PDEs. As a result, one must decide if this is ultimately a good trade or not.

Since the proposed preconditioner is not unique and the original 5-moment system can have many effective preconditioners, one could try to develop a preconditioner that might result in a conservative system, such that $\mathbf{P}\frac{\partial \mathbf{F}}{\partial \mathbf{U}} = \frac{\partial \mathbf{G}}{\partial \mathbf{U}}$ where $\mathbf{G}$ is the flux vector of the new preconditioned 5-moment system. Unfortunately, experience has shown that the construction of such a preconditioning matrix is extremely difficult.

The applicability of results in this work are restricted to one-dimensional gases. For realistic three dimensional applications, techniques developed here would have to be extended to the full equivalent fourteen-moment system that is the three-dimensional corollary of the five-moment model used herein. The fourteen-moment flux Jacobian shows many similarities to the one studied in this work. It is likely that many ideas used here can be extended to the higher-dimensional system.

References

[1] P. L. Bhatnagar, E. P. Gross, and M. Krook. A model for collision processes in gases. I. small amplitude processes in charged and neutral one-component systems. *Physical Rev.*, 94(3):511–525, 1954.

[2] G. A. Bird. *Molecular Gas Dynamics and the Direct Simulation of Gas Flows*. Clarendon Press, Oxford, 1994.

[3] A. Canestrelli, A. Siviglia, M. Dumbser, and E. F. Toro. Well-balanced high-order centred schemes for non-conservative hyperbolic systems. applications to shallow water equations with fixed and mobile bed. *Elsevier*, 2009.

[4] S. Chapman and T. G. Cowling. *The Mathematical Theory of Non-Uniform Gases*. Cambridge University Press, Cambridge, 1970.

[5] A. J. Chorin. A numerical method for solving incompressible viscous flow problems. *J. Comput. Phys.*, 2(1):12–26, 1967.

[6] W. J. Coirier. *An Adaptively-Refined, Cartesian, Cell-Based Scheme for the Euler and Navier-Stokes Equations*. PhD thesis, University of Michigan, 1994.

[7] Edgar Dehn. *Algebraic Equations: An Introduction to the Theories of Lagrange and Galois*. Columbia University Press, 1930.

[8] A. G. Godfrey, R. W. Walters, and B. van Leer. Preconditioning for the Navier-Stokes equations with finite-rate chemistry. Paper 93-0535, AIAA, January 1993.

[9] S. K. Godunov. Finite-difference method for numerical computations of discontinuous solutions of the equations of fluid dynamics. *Mat. Sb.*, 47:271–306, 1959.

[10] T. I. Gombosi. *Gaskinetic Theory*. Cambridge University Press, Cambridge, 1994.

[11] H. Grad. On the kinetic theory of rarefied gases. *Commun. Pure Appl. Math.*, 2:331–407, 1949.

[12] H. L. Hamburger. Hermitian transformations of deficiency-index $(1, 1)$, jacobian matrices, and undetermined moment problems. *Amer. J. Math.*, 66:489–552, 1944.

[13] M. Junk. Domain of definition of Levermore's five-moment system. *J. Stat. Phys.*, 93(5/6):1143–1167, 1998.

[14] G. M. Kremer. *An Introduction to the Boltzmann Equation and Transport Processes in Gases*. Springer-Verlag, Berlin, 2010.

[15] C. K. S. Lam and C. P. T. Groth. Numerical prediction of three-dimensional non-equilibrium gaseous flows using the Gaussian moment closure. Paper 2011-3401, AIAA, June 2011.

[16] R. J. LeVeque. *Finite Volume Methods for Hyperbolic Problems*. Cambridge University Press, New York, 2002.

[17] C. D. Levermore. Moment closure hierarchies for kinetic theories. *J. Stat. Phys.*, 83:1021–1065, 1996.

[18] J. G. McDonald. *Extended Fluid-Dynamic Modelling for Numerical Solution of Micro-Scale*. PhD thesis, University of Toronto, October 2010.

[19] J. G. McDonald and A. R. Baradaran. A robust and efficient unified model for continuum and transition-regime flow prediction. In *The Eighth International Conference on Computational Fluid Dynamics (ICCFD8), Chengdu, Sichuan, China, July 14-18, 2014*, 2014.

[20] J. G. McDonald, J. S. Sachdev, and C. P. T. Groth. Application of Gaussian moment closure to micro-scale flows with moving and embedded boundaries. submitted to the AIAA Journal, January 2013.

[21] J. G. McDonald and M. Torrilhon. Affordable robust moment closures for CFD based on the maximum-entropy hierarchy. *J. Comput. Phys.*, 251:500–523, 2013.

[22] L. Mieussens. Discrete velocity model and implicit scheme for the BGK equation of rarefied gas dynamics. *Mathematical Models and Methods in Applied Sciences*, 10(8):1121–1149, 2000.

[23] I. Müller and T. Ruggeri. *Rational Extended Thermodynamics*. Springer-Verlag, New York, 1998.

[24] Carlos Pares. Numerical methods for nonconservative hyperbolic systems. *SIAM J. NUMER*, pages 300–321, 2003.

[25] K. Friedrichs R. Courant and H. Lewy. On the partial difference equations of mathematical physics. *Mathematishe Annlen*, pages 32–74, 1928.

[26] H. Struchtrup. *Macroscopic Transport Equations for Rarefied Gas Flows*. Springer-Verlag, Berlin, 2005.

[27] Y. Suzuki and B. van Leer. Application of the 10-moment model to MEMS flows. Paper 2005-1398, AIAA, January 2005.

[28] E. F. Toro and A. Siviglia. Price: primitive centred schemes for hyperbolic systems. *Interntional Journal for Numerical Methods in Fluids*, pages 1263–1291, 2003.

[29] M. Torrilhon. Characteristic waves and dissipation in the 13-moment-case. *Continuum Mech. Thermodyn.*, 12:289–301, 2000.

[30] M. Torrilhon. Hyperbolic moment equations in kinetic gas theory based on multivariate Pearson-IV-distributions. *Commun. Comput. Phys.*, 7(4):639–673, 2010.

[31] E. Turkel. Preconditioning techniques in computational fluid dynamics. *Ann. Rev. Fluid Mech.*, 31:385–416, 1999.

[32] J. M. Weiss and W. A. Smith. Preconditioning applied to variable and constant density flows. *AIAA J.*, 33(11):2050–2057, 1995.